Master Thesis: Quantifying the Anthropogenic Methane Emission from Large Local Sources

Author: Han Chen[1,2]

Supervisors: Sander Houweling[1,2], Rob Detmers[2], Thomas Röckmann[1]

[1]Utrecht University, Heidelberglaan 8, NL-3584 CS Utrecht, Netherlands
[2]SRON Netherlands Institute for Space Research, Sorbonnelaan 2, NL-3584 CA Utrecht, Netherlands

14th August 2017

Abstract

Methane is a potent greenhouse gas. The aim of the project is to quantify anthropogenic emissions of methane from large local sources, such as cities and industrial facilities using satellite data. Of scientific interest is the comparison of methane emissions estimated using top down (satellite) and bottom up (statistical inventories) approaches. We make use of satellite data from SCIAMACHY. In an earlier master research project, a new local methane emission hotspot is found in South Shānxī Province, China with the satellite data, which is not shown in EDGAR version 4.2, but added in the latest EDGAR draft version 4.3.2. Together with a well validated methane hotspot in Four Corners, USA, the methane emissions of these two hotspots are studied in this research. China has complicated local anthropogenic methane emission sources, but without a precise measurement inventory. In this research, based on TM5 simulated data, a global orographic correction matrix is developed and applied to eliminate the influence of elevation variations, which theoretically gets rid of the influences of potential anthropogenic sources better than the old elevation correction method. A new gridding way is constructed and applied on both Four Corners and South Shānxī source areas to experiment on the effects of gridding methods. The new gridding method shows no significant difference, which proves the robustness of the emission estimation results. The latest EDGAR draft version 4.3.2 is applied, which includes the updated coal mine maps. The quantification results in Four Corners keep consistent, and show the EDGAR draft v4.3.2 in SS is possible to be overestimated.

Contents

1. Introduction

Methane (CH_4) is a potent greenhouse gas and ozone precursor (*Kort et al., 2014*). Since 1750, the methane concentration in the Earth's atmosphere has increased by about 150%, which causes global warming and contributes about 20% to the combined radiative forcing from all long-lived and globally well mixed greenhouse gases (excluding water vapor) (*IPCC, 2001*). To gain a better understanding, we could either consider the processes and compile the available information (e.g. The Emissions Database for Global Atmospheric Research (hereinafter EDGAR) emission inventory) or try to quantify emissions using atmospheric data. The use of atmospheric data is a way to independently verify the inventories. The Paris Agreement urges countries to reduce carbon emissions. However, we need a system capable of checking whether countries keep up with their promises. Satellite measurements are a crucial step towards that goal. Several missions are designed to map local sources from both governmental agencies and companies. SRON is preparing for the launch of the Dutch instrument TROPOMI. That instrument will also allow important steps forwards. However, in preparation for that, useful analyses of satellite data can already be done using SCanning Imaging Absorption spectroMeter for Atmospheric CHartographY (hereinafter SCIAMACHY). The SCIAMACHY was launched on board ENVISAT, which was operational from March 2002 to April 2012 (*http://www.sciamachy.org/*), with accessible methane products.

In this research, we will use top-down (satellite data) and bottom-up (statistical inventories) approaches to quantify methane emissions from large local sources found in Four Corners, U.S. (hereinafter 4C) and South Shānxī, China (hereinafter SS). Methane emissions from the 4C mining region were investigated by *Kort et al. (2014)* who found that emissions derived using SCIAMACHY satellite data were a factor of 3.5±0.5 (2σ) larger than in the EDGAR v4.2 inventory for 2008. Emissions obtained using SCIAMACHY (0.59 $Tg \cdot yr^{-1}$, (0.50~0.57, 2σ)) are supported by local ground-based measurements as part of TCCON (Total Carbon Column Observing Network) (*Wunch et al., 2011*).

Using SCIAMACHY data, another large local methane emission source was found in SS in the thesis of *Jens Wagemaker (hereinafter J. W.) (2016)*, who determined an emission of 0.31± 0.14 $Tg \cdot yr^{-1}$ for this source. Initially, this source was not present in the EDGAR v4.2 inventory. Meanwhile, updated maps are used in EDGAR for disaggregating Chinese emission statistics available at the provincial and national level. The latest version (EDGAR draft v4.3.2 2008 inventory) does show a large local emission ($4.19 \times 10^{-9}\ kg \cdot m^{-2} \cdot s^{-1}$) around the hotspot that was detected using SCIAMACHY.

The aim of this study is to further improve the emission quantification using satellite data. To reach this goal, a new global orographic correction method is developed based on the global atmospheric chemistry Transport Model (hereinafter TM5 model). It is used to decrease the influence of local surface elevation variations. In the method of *J. W. (2016)*, this influence is difficult to be separated from anthropogenic sources in the regions surrounding the interested hotspots. This is important in particular when addressing local emissions in highly industrialized and densely populated regions, which are common in China. In addition, a new regridding method is developed for improved mapping of multi-year average SCIAMACHY data.

This report consists of five parts: introduction, methods, results, conclusions and discussions. The method part includes the input datasets and explains the mechanisms of gridding, elevation correction, emission estimation, target emission and area selection. The result part shows the elevation correction matrix and emission estimation.

2. Methods

2.1. Input Datasets

2.1.1. SCIAMACHY Satellite Instrument

General Introduction

SCIAMACHY is a passive remote sensing spectrometer observing backscattered, reflected or transmitted radiation from the atmosphere and Earth's surface, in the wavelength range between 240 and 2380 nm. The instrument was launched on board ENVISAT which was operational from March 2002 to April 2012. (*Bovensmann et al., 1999*)

The primary scientific objective of SCIAMACHY is the global measurement of various trace gases in the troposphere and stratosphere, which are retrieved from the solar irradiance and Earth radiance spectra. The large wavelength is also ideally suited for the determination of aerosols and clouds. Validation of SCIAMACHY is essential to ensure the quality of these derived products. (*http://www.sciamachy.org/*)

SCIAMACHY has three different viewing geometries: nadir, limb, and sun/moon occultations which yield total column values as well as distribution profiles in the stratosphere and (in some cases) the troposphere for trace gases and aerosols. (*http://earth.esa.int/*)

The equipment is on the sun-synchronous orbit, crossing the equator at 10:00 am. The nadir footprint is ~30 km (along track) × 60 km (across track) depending on species. The swath width is 960 km swath with variable integration periods, ~30 km along track. It attains global coverage in ~6 days. SCIAMACHY measures methane at 1.6 microns. The measurements both within and outside the methane absorption band allow one to determine both the methane optical depth and the surface albedo, which does not vary strongly over a narrow wavelength interval. There are few measurements over the ocean due to low albedo. (*ftp://ftp.bgc-jena.mpg.de/*)

Total Column CH_4 (XCH_4)

The matric for atmospheric CH_4 concentrations used in the research is the column averaged mole fraction (of CH_4 and dry air) denoted by XCH_4, it is the ratio between the Vertical Column Densities of CH_4 and dry air, as is expressed in Equation 1. This quantity is retrieved from the

SCIAMACHY observed spectra using the so called 'proxy' approach. The wavelength used for retrieving CH_4 is 1.6 mircons which is a main reason why the proxy method works well, since CO_2 and CH_4 absorb at wavelengths that are spectrally very near to each other. Because of this, aerosol scattering affects CO_2 and CH_4 in a very analogous manner, which is in a way that cancels out in the proxy ratio. The advantage of this retrieval method is that is that it accounts for the influence of aerosols and clouds on the light path in a highly efficient manner (*Frankenburg et al., 2016*). The proxy method uses the following equation

$$\mathrm{XCH_4} = \frac{\mathrm{VCD\_CH_4}}{\mathrm{VCD\_air}} = \frac{\mathrm{VCD\_CH_4}}{\mathrm{VCD\_CO_2}} \cdot \mathrm{XCO_2\_model} \quad (1)$$

where XCO_2 was obtained from the Carbon Tracker 2011 model (*Peters et al., 2007*).
When researching total column CH_4, the vertical sensitivity (i.e. the averaging kernel) needs to be considered. Averaging kernels describe how the sensitivity of a remote CH_4 measurement varies with height. This sensitivity varies due to the interaction of spectroscopy and radiative transfer with atmospheric properties, and to instrument optical characteristics and spectral response. So, the profile shape and variability with height affects the retrieved column and its comparison to models and other measurements.

SCIAMACHY Data Products

The data product used here is the IMAP_DOAS XCH_4 SCIAMACHY Data Product (v7.2). It contains all useful XCH_4 measurements (e.g. cloud-free, good spectral fit) retrieved from SCIAMACHY in the period from 2003 to 2012. The data is stored in daily files in the NetCDF (Network Common Data Form) format (*Rew and Davis, 1990*). The time range used in this research is from 2003 – 2009, to keep consistent with the research of *Kort et al. (2014)* who studied methane emission in the 4C region in the USA. The variables used are listed in Table 1.

Table 1. Variables from IMAP-DOAS XCH_4 SCIAMACHY Data products (v7.2) that were used in this research.

variable	dim	long name	units	comment
ch4_profile_apriori	10 (layer_dim)	a priori profile of dry-air mole fraction of atmospheric methane	ppb	a priori profile of dry-air mole fraction of atmospheric methane (XCH_4)
latitude		latitude	degrees_north	Center latitude of the measurement
latitude_corners	4 (corner_dim)	latitude_corners	degrees_north	Latitude corners of the measurement
longitude		longitude	degrees_east	Center longitude of the measurement
longitude_corners	4 (corner_dim)	longitude_corners	degrees_east	Longitude corners of the measurement
pressure_levels	11 (layer_dim)	pressure levels	hPa	Pressure levels define the boundaries of the averaging kernel and mole fraction profile layers. Surface pressure is represented by the 1st element, i.e., profiles are ordered from surface to top of atmosphere.
surface_elevation		Height	m	Height is the vertical distance above the surface
time		time	seconds since 1970-01-01 00:00:00	
xch4		column-average dry-air mole fraction of atmospheric methane	ppb	Bias-corrected retrieved column-average dry-air mole fraction of atmospheric methane (XCH_4)
xch4_averaging_kernel	10 (layer_dim)	normalized column averaging kernel	1	The normalized column-averaging kernel represents the sensitivity of the retrieved XCH_4 to the atmospheric methane mole fraction depending on pressure (height). All values represent layer averages within the corresponding pressure levels. Values near one are ideal and indicate that the influence of the a priori is minimal. Profiles are ordered from surface to top of atmosphere.
xch4_uncertainty		1-sigma uncertainty of the retrieved column-average dry-air mole fraction of atmospheric methane	ppb	detector noise-driven 1-sigma uncertainty of the retrieved column-average dry-air mole fraction of atmospheric methane (XCH_4) in ppb

2.1.2. TM5 Model

TM5 is a global atmospheric chemistry transport model, with the unique capability to zoom over specific areas (*Krol et al., 2005*). The model is off-line and uses meteorological fields from the European Centre for Medium Range Forecasting (ECMWF) ERA Interim re-analysis. This research makes use of the results of a TM5 simulation of global CH_4, at a horizontal resolution of 3° × 2° (longitude × latitude) and 36 vertical levels from the surface to the top of the atmosphere. The data are stored in daily NetCDF files for the year 2010. The variables used are shown in Table 2.

Table 2. Variables from TM5 model dataset that were used in this research.

variable	levels (or boundaries)	long name
gph	37	geopotential height (in meters) at the level boundaries
mix	36	mixing ratio (in this paper it is called mole fraction)
pressure	37	pressure (in Pa) at the level boundaries

Concentrations of CH_4 as measured by SCIAMACHY cannot be translated directly to actual emissions of CH_4 at the surface. For this we need an atmospheric transport model in which emissions are prescribed as boundary conditions and the atmospheric dispersion and chemical transformation processes are calculated, yielding the impact of surface emissions on the atmospheric mole fraction of CH_4. Since atmospheric tracer transport is linear, the response of a unit emission pulse can simply be scaled to fit observed concentration enhancements. This way an estimate of surface emissions can be obtained given a satellite observed local enhancement in XCH_4. The atmospheric oxidation of methane is taken into account in the model, but does not play a role when estimating local emissions, because of the long lifetime of methane in the atmosphere ($\tau \approx 10$ years, *Patra et al., 2011*).
To get first order estimates of emissions corresponding to SCIAMACHY observed hotspots in CH_4, we use the global chemistry transport model TM5.
This research focuses on local 'hotspots' of enhanced XCH_4 caused by local sources. These hotspots are modeled as point sources, however, because of the limited resolution of the model, these correspond to uniform emissions over a single grid-cell of 1° × 1°, or approximately 100 × 100 km^2 depending on the geographical location.

2.1.3. Inventory Emissions

In our research, we need a bottom-up inventory for the methane emission estimation in the target areas. The Emissions Database for Global Atmospheric Research (EDGAR) provides global past and present day anthropogenic emissions of greenhouse gases and air pollutants by country and on a spatial grid (*http://edgar.jrc.ec.europa.eu/*). In the previous research of *J. W. (2016)*, the version 4.2 is applied. However, now a new draft version 4.3.2 is accessible (*ftp://ftp-ccu.jrc.it/*), which contains more accurate anthropogenic emission inventories for

the interested area around the hotspot found in SS. The datasets used in this research are of year 2008. Since the EDGAR draft v4.3.2 inventory is still a draft version, after comparing with the published EDGAR v4.2, the 'large scale biomass burning' term is added from v4.2. The rest terms used in emission estimations are all from draft v4.3.2. The term 'total' is the sum of all emission processes.

Table 3. EDGAR draft v4.3.2 inventory.

Abbreviation	Full name	IPCC code
AGS	Agricultural soils	4C, 4D
AWB	Agricultural waste burning	4F
CHE	Production of chemicals	2B
ENE	Energy industry	1A1a
ENF	Enteric fermentation	4A
FFF	Fossil fuel fires	7A
IND	Manufacturing Industry	1A2
IRO	Production of iron and steel	2C1a, 2C1c, 2C1d, 2C1e, 2C1f, 2C2
LBB (from EDGAR v4.2)	Large scale biomass burning	5A, 5C, 5D, 5F, 4E
MNM	Manure management	4B
PRO	Fuel combustion and production	1B1a, 1B2b, 1B2c, 1B2a, 1B2c
RCO	Residential	1A4
REF_TRF	Oil refineries, transformation industry	1A1b, 1A1c, 1A5b1, 1B1b, 1B2a5, 1B2a6, 1B2b5, 2C1b
SWD	Solid waste disposal	6C, 6A, 6D
TNR	Non-road transport	1A3a, 1A3c, 1A3e, 1A3d, 1C2
TRO	Road transport	1A3b
WWT	Waste water	6B

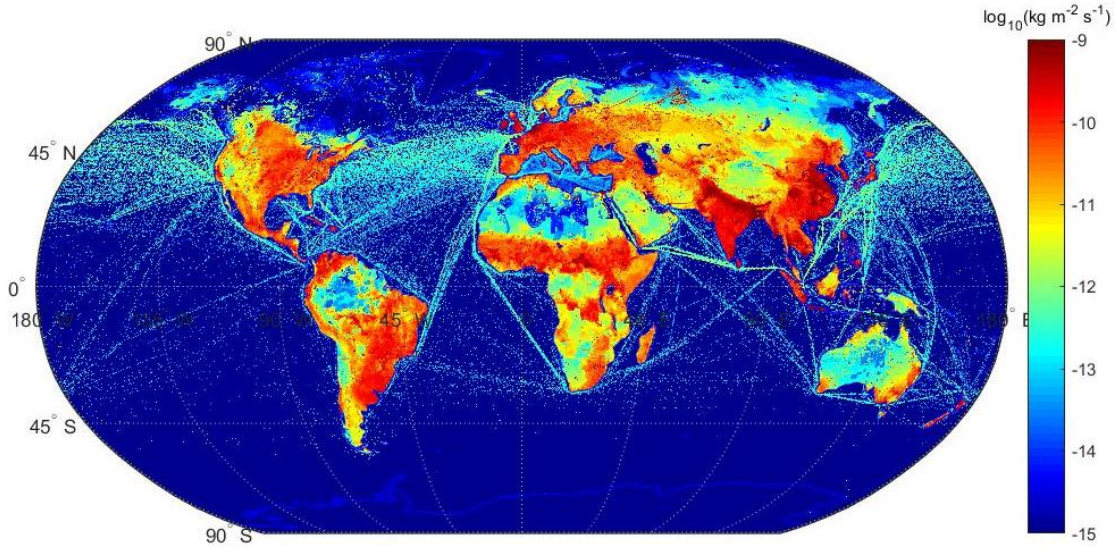

Figure 1. Global CH_4 emissions from the EDGAR draft v4.3.2 emission inventory for the year 2008 at a spatial resolution of 0.1°×0.1°.

2.2. Methodology

2.2.1. Gridding of Satellite Data

For the analysis of SCIAMACHY data, the earth surface is gridded in regular lon/lat projection at resolutions of 1°×1°. The time range in the analyses is from 2003 to 2009, in order to keep consistent with the validation of the research of *Kort et al., 2014*.
The mean and uncertainty in multi-annual and grid averaged XCH_4 is calculated as follows:
For each daily file, there are multiple columns with XCH_4 and uncertainty data:
XCH_4 of column i: x_i, uncertainty of column i: σ_i.
The weight of each column is calculated based on uncertainty:

$$\text{weight: } w_i = \frac{1}{\sigma_i^2} \tag{2}$$

We take the center lon/lat location as which grid cell the data in the column belong to. For each grid cell, the XCH_4 and uncertainty data are calculated as follow:

$$\text{uncertainties calculated from weights: } \sigma_{wav} = \sqrt{\frac{1}{\sum_i w_i}} \tag{3}$$

$$\text{mole fraction: } x_{wav} = \frac{\sum_i w_i x_i}{\sum_i w_i} \tag{4}$$

With various daily weighted-average data for 7 years, the weighted average-all-time XCH_4 and uncertainty data are calculated as:

$$\text{weight: } w_{wav} = \frac{1}{\sigma_{wav}^2} \tag{5}$$

$$\text{uncertainties calculated from weights: } \sigma_{avg\_all\_time} = \sqrt{\frac{1}{\sum w_{wav}}} \tag{6}$$

$$\text{mole fraction: } x_{avg\_all\_time} = \frac{\sum w_{wav} x_{wav}}{\sum w_{wav}} \tag{7}$$

The advantage of calculating weighted average-all-time data is to decrease the influence of the data with uncertainties. When calibrating the elevation correction matrix derived from TM5 model in Section 3.1, weighted average-day is calculated in the same way as Equation 5 - 7.

For exploring the effects of different gridding methods, a new gridding method is applied in this research. In the gridding method described above, the data of each column fall into one grid cell fully depend on the center lon/lat location. However, because of the irregular shapes of the data footprints, there is a possibility that one data column can stand for various grid cells. Now we want to develop a new gridding method, which takes the shape of data footprint into consideration. The purpose is to test out a method which ought to be more precise than what was done before, and to test the sensitivity of the outcome to the averaging method.

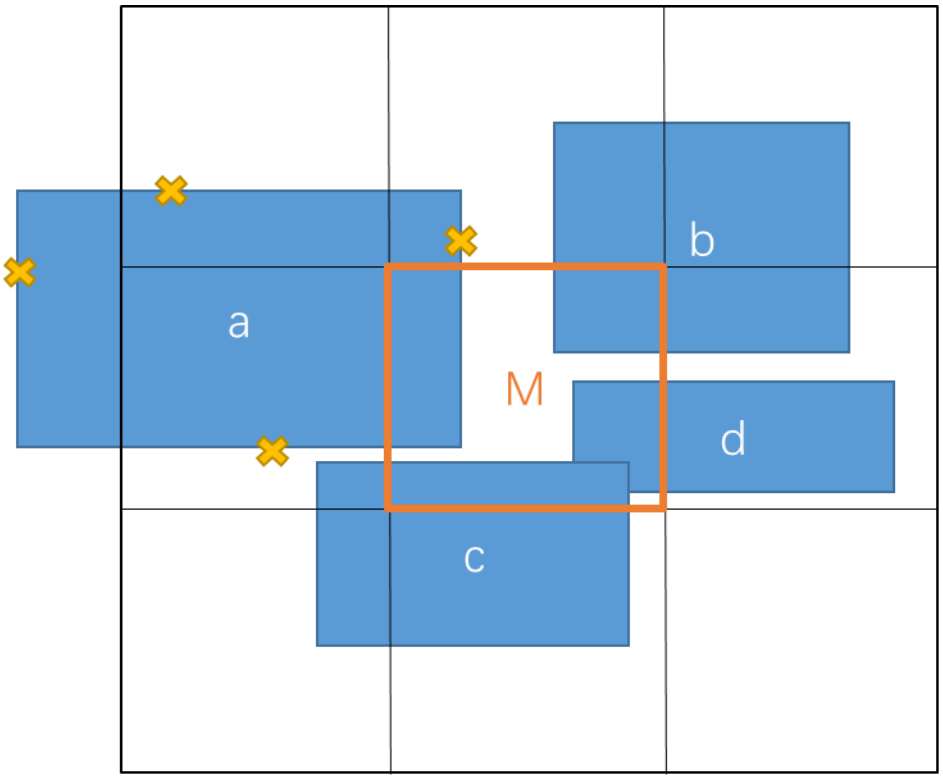

Figure 2. Illustration of the re-gridding method.

As shown in Figure 2, the shape of each data point is approximated as a rectangle, e.g. in a. For the overlapped area, e.g. in a, the XCH_4 and uncertainty values are considered to be the same in the data column a, which are $x_i = x_a,\ \sigma_i = \sigma_a$
However, we define a ratio for the overlapped area of a and M:

$$r_i = \frac{S_{overlapping}}{S_M} \tag{8}$$

Then the weight of the overlapped area of a and M in grid cell M is

$$w_i = \frac{r_i}{\sigma_i^2} \tag{9}$$

For the grid box M, the XCH_4 and uncertainty values are calculated as follow:

$$XCH_{4_M} = \frac{\sum w_i x_i}{\sum w_i} \tag{10}$$

$$\sigma_M = \sqrt{\frac{\sum r_i}{\sum w_i}} \tag{11}$$

With the new gridded daily files of data, the weighted average-all-time XCH_4 and uncertainty values are calculated as Equation 5 - 7. When calibrating the elevation correction matrix derived from TM5 model in Section 3.1, weighted average-day is calculated in the same way as Equation 5 - 7.

2.2.2. Elevation Correction

The height of the tropopause determines the weights of the troposphere and the stratosphere in calculating XCH_4 (column averaged mole fraction). The CH_4 abundance is lower in the stratosphere than in the troposphere, as can be seen in Figure 3, which is due to slow mixing in the stratosphere and photochemical destruction of methane in reaction with OH, $O(^1D)$ and Cl radicals as well as a minor contribution from photolysis (*Frankenberg et al., 2011*). In the SCIAMACHY data, this lower abundance of methane in the stratosphere causes a negative correlation between the surface elevation and XCH_4. The reason is that surface elevation causes a reduction in the mass of the tropospheric sub-column. Therefore, a change in surface elevation causes a shift in the contribution of the tropospheric and stratospheric air mass to the total column. As a result, XCH_4 decreases as surface elevation increases, which makes it necessary to take the effect of elevation into account when estimating CH_4 emissions.

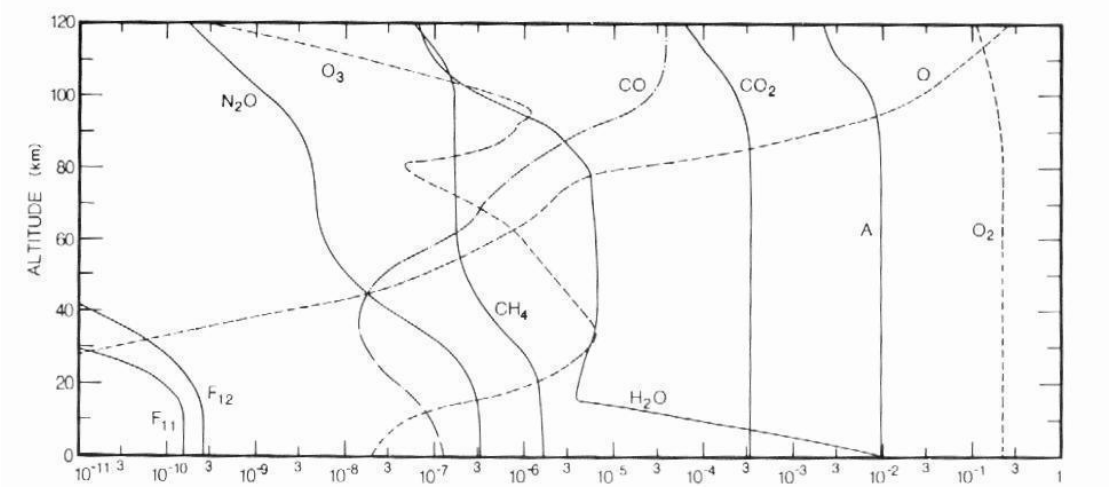

Figure 3. Vertical profiles of the mole fractions of selected species at the equinox. (From *Goody and Yung, 1989*)

Because of the 'elevation effect', we perform the elevation correction to get rid of the influence from the surface elevation variation in the process of emission quantification. In the

previous work of J. W., 2016, an elevation correction method is applied based on the SCIAMACHY data around the source region. It works relatively well in regions with simple emission inventories, for example 4C and Middle East. However, in this research, SS hotspot is surrounded by highly industrialized areas, with a lot of unknown local methane emission sources. To get rid of the potential influences from the surrounding local sources, we intend to construct a new global elevation correction method, with the help of TM5 model. In TM5 the height dependence is calculated in a different way, which is not sensitive to the presence of local emissions.

From Figure 3, we assume there is a first order linear relationship between the surface elevation and the methane mole fraction. This linear relationship is determined by a linear regression between the methane mole fraction and the surface elevation. However, since TM5 model has 36 layers, up to 200 km above the earth surface, we need a method to derive the elevation correction near the surface, i.e. for the range of surface elevation changes relevant for the SCIAMACHY data. When extending the range to higher elevations in the model, deviations from linearity become important deteriorating the accuracy of the elevation correction.

Our method of elevation correction is described in the following. For each layer, the methane mole fraction (*mix:* i ··· 36) is used, as well as the geopotential height (*gph:* i ··· 37) and pressure (*p:* i ··· 37) at each layer boundary.

For each layer, the pressure difference is

$$d\_p_i = p_i - p_{i+1} \tag{12}$$

In the layers above boundary *i,* the methane mole fraction is calculated

$$mix_{above} = \frac{\sum_i^{36} mix_i \cdot d\_p_i}{\sum_i^{36} d\_p_i} \tag{13}$$

When we do the elevation correction for TM5, we would only keep the mix_{above} values from 0 to 3 km above the earth surface. Since when it comes to higher altitudes, the linear relation of methane mole fraction and surface elevation disappears. Also, because SCIAMACHY data points are mostly less than 3 km above the earth surface, which is consistent if we only take mix_{above} values from 0 to 3 km above the surface.

The regression yields the function:

$$XCH_4 = slope \times elevation + intercept \tag{14}$$

where the slope and intercept are obtained for each area that is to be corrected for elevation. The actual correction was performed by replacing the XCH_4 of each measurement by $XCH_4 - slope \times surface\_elevation$, where *slope* comes from the selected elevation correction area.

In this research, elevation corrections are done for data from both TM5 model and SCIAMACHY. In TM5 model elevation correction, the regions are defined freely. Since our aim

is to construct a global elevation correction matrix, and the model results are available everywhere on earth without the influence of unknown local emission sources. But in SCIAMACHY elevation correction, we need to look for proper defined regions to apply the elevation correction for deriving better slope values, which are regions with few industries, little cloud coverages and big elevation variations. When applying the elevation correction to SCIAMACHY, we define three different regions surrounding the local methane source of interest. The small region in the direct vicinity of the source, a larger region encompassing the small region, and an even larger region encompassing the middle region. The smallest region has an advantage that the regression is more representative of the location of the local source. When applying the method to SCIAMACHY data we choose targets that are surrounded by regions where the emissions are low according to the emission inventory (as is the case in the 4C region). As a result, XCH_4 variations at some distance of the source reflect mostly altitude variations. The largest region has most data-points and therefore the statistical error of the regression should be smallest. However, large regions commonly also include regions with substantial methane emissions, contaminating the relation between XCH_4 and elevation. After doing the linear regression for each of the 3 regions, we calculate and compare the root mean squares (*rms*) and select the area with the smallest *rms* number.

$$rms = \sqrt{\frac{\sum_{i=1}^{n} r^2}{n}} \tag{15}$$

Where *r* is the distance of every data point to the linear regression line in the vertical direction. Regions with a large *rms* either have data shortage, or are substantially influenced by regional emissions.

In the previous work done by J. W., 2016, he applies a simple and direct elevation correction method which does not consider the influences of latitude, longitude and seasonal variations. But it is not valid for this research for the main target is in China, where J. W.'s approach does not work well because of the unknown local emissions. In the 4C hotspot, the surrounding emissions are small with reliable local emission measurements, e.g. TCCON. But in SS hotspot, the surrounding emissions are complicated and unclear. This is the reason why a global elevation correction method is constructed in this research.

Since the contribution of the stratospheric and tropospheric sub columns varies around the globe, the elevation correction is expected to be different for different regions and seasons. The tropopause is usually found around 12 km, although it is somewhat higher in the tropics and lower in the polar regions. The height of the tropopause also varies with season owing to changes in the atmospheric circulation. (*http://www.ccpo.odu.edu/*). Therefore, in this research the seasonal and latitude variation of elevation correction are studied to construct a better method to do the elevation correction, that can be applied anywhere on the globe.

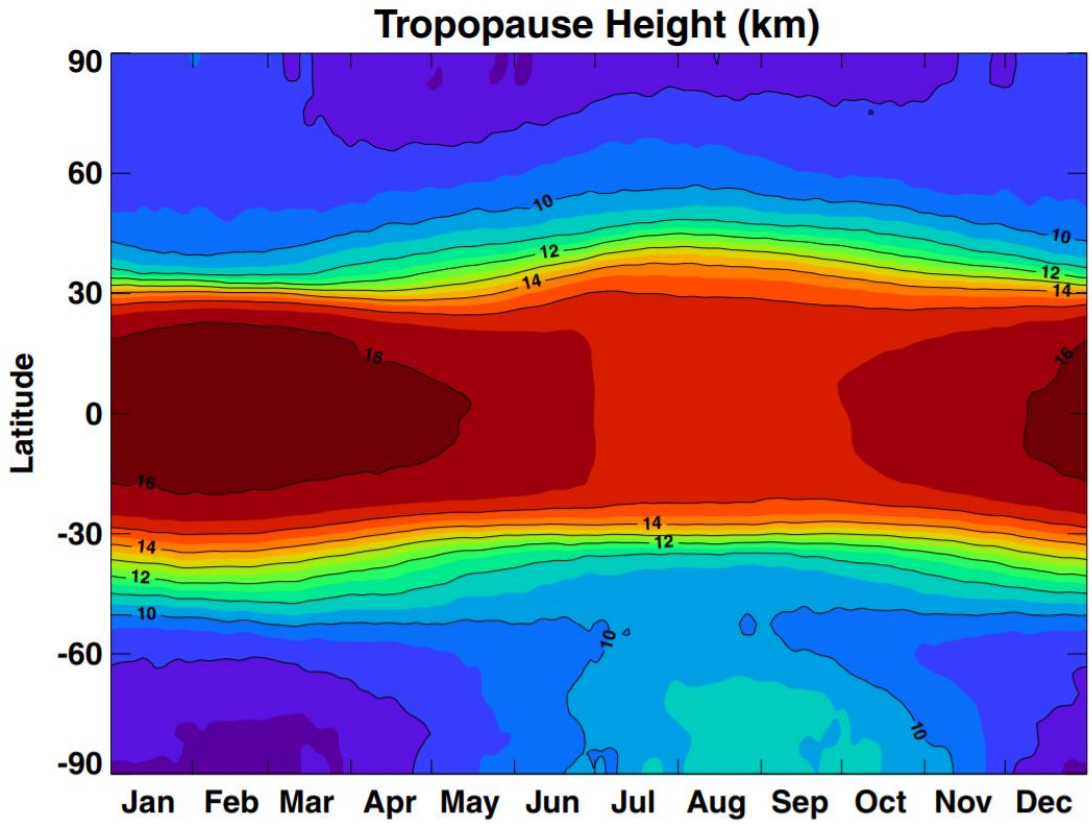

Figure 4. Tropopause as a function of latitude with seasonal variations. (From *http://www.ccpo.odu.edu/*)

The advantage of using TM5 model instead of SCIAMACHY data to construct the elevation correction method, is that we can derive a global elevation correction map, which is not limited by the availability of SCIAMACHY, thus avoiding the influence of land-ocean coverage, latitude variations etc. However, the elevation correction matrix derived from the TM5 model will have to be validated to make sure that it correctly represents the altitude dependence of XCH_4 in the SCIAMACHY data. For this purpose, we make use of regions where reliable altitude corrections can be derived from the SCIAMACHY data. Examples are regions without important surface emissions, and limited cloud cover, such as the 4C region (i.e. the region surrounding the large local source), the Middle East and the Sahara. Finally, the validated global elevation correction matrix from TM5, fine-tuned using SCIAMACHY, is used to carry out the elevation correction for the hotspot in SS. This way, the elevation correction avoids the influence of local sources, improving the accuracy of the derived emissions.

2.2.3. Background Selection and ΔXCH_4

As explained earlier, the methane emission from local sources as quantified by the difference in XCH_4 between the target and its surroundings, as follows:

$$\Delta XCH_4 = XCH_{4_{source}} - XCH_{4_{background}} \quad (16)$$

The difficult part is to determine a representative background methane mole fraction. Using the elevation correction, we account for an important source of XCH_4 variation in the background. However, in source regions, like in China, significant XCH_4 variability remains at distance of the target source. In this research, we define the background of the source as the neighboring grid-cells around the hotspot with the lowest mole fraction values. This supported by the notion that surface fluxes of methane are predominantly sources, and therefore the lowest columns represent air that is influenced the least by local emissions. For each hotspot, three varied sizes of background regions are chosen, with the smaller regions progressively zooming into the vicinity of the target. The trade-off in region size follows the same logic as for the altitude correction: it is a balance between number of data and representativeness of local conditions. It was found that the ΔXCH_4 calculated using different backgrounds fall within each other's error range for all hotspots. However, the large regions get the smallest uncertainties (*J. W., 2016*). So, in this research we choose the large sizes of background regions for calculations.

2.2.4. Emission Quantification

The following equation is used for deriving the emission difference between the hotspot and the background:

$$\frac{\Delta EMI}{\Delta XCH_4} = \frac{\Delta EMI\_TM5}{\Delta XCH_4\_TM5} \tag{17}$$

In the left-hand side, ΔXCH_4 is the difference between the hotspot and the background, which can be obtained from the elevation corrected SCIAMACHY data. In the right-hand side, ΔEMI_TM5 is preset to 1 Tg·yr^{-1} for all simulations; ΔXCH_4_TM5 is the quantity retrieved by performing the forward run with the TM5 model. The two variables on the right-hand side are obtained from the TM5 model. Equation 17 is used to derive ΔEMI. EMI_source or simply EMI is the quantity of interest, which represents the emission of the source/hotspot.

$$EMI_{source} = \Delta EMI + EMI_{background} \tag{18}$$

In Equation 18, $EMI_{background}$ is derived from EDGAR draft v4.3.2, combining the information from all source processes. With all this information available we can obtain an estimate of EMI_{source}.

Since there is no uncertainty available in the EDGAR inventory, the uncertainty of EMI_{source} is set to be the same as $EMI_{background}$. The uncertainty of $EMI_{background}$ is calculated from gridded SCIAMACHY data of all the background grid cells chosen in Section 3.1.

2.2.5. Validation to Four Corners Region

The process described above has various uncertainties and needs to be calibrated. Because:

1. TM5 is a global model, which might not be suitable for analysis on the local scale.
2. The idealized model simulation might be too simple, since there are other sources outside the area that was marked source area.
3. For the absolute emission of the background EDGAR 'Total' was used, but this does not contain natural emissions, which is principally not applicable for China.
4. The emission simulations are performed for the year 2008, but the SCIAMACHY data used are from 2003 to 2009. However, EDGAR emissions in the 4C region change little both spatially and in magnitude from year to year (*Kort et al., 2014*).

Therefore, a validation of our method is required, for which we use the study by *Kort et al. (2014)*. In *Kort et al., 2014*, they present CH_4 observations made from space combined with Earth-based remote sensing column measurements. After calculating the linear coefficient of simulated enhancement (WRF-Chem) and SCIAMACHY observed enhancement, a slope of 3.5±0.5 (2σ) is determined. With the determined coefficient as correction number of EDGAR emissions around 4C region (from -109.6°W to -107.0°W and 36.2°N to 37.4°N), the emission is concluded as 0.59 Tg CH_4 yr^{-1} (0.50-0.67; 2σ). It agrees with the results of ground-based validation from TCCON observations.

However, this emission is calculated for a partially different area than the source-area used here as is shown in Figure 5. The version of the EDGAR dataset used in the paper is also different from draft version 4.3.2 used here. These factors complicate the comparison and call for a more detailed analysis.

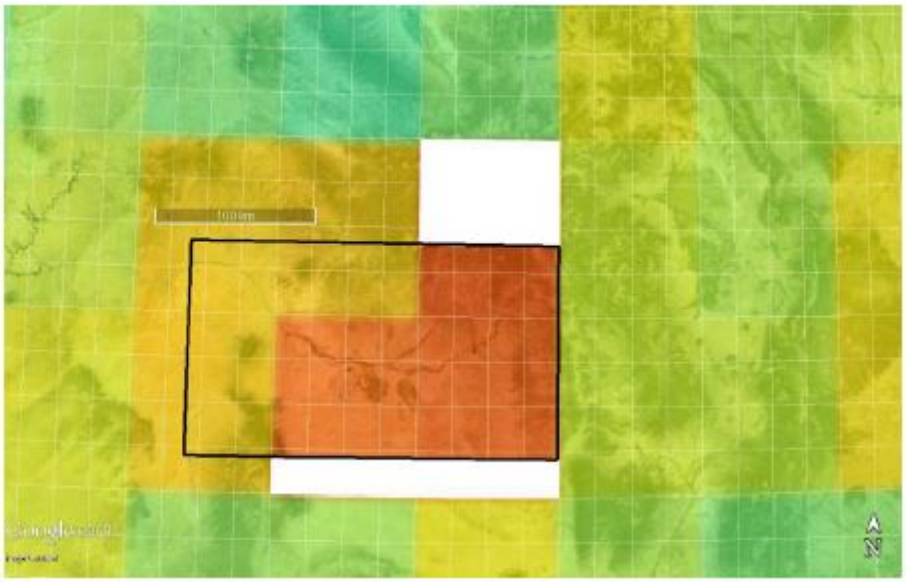

Figure 5. shows the 4C hotspot area used here in orange and white, and the 4C area used by (*Kort et al., 2014*) in the black rectangle. (from *J. W., 2016*)

Kort et al. (2014) derive an upward correction of the EDGAR v4.2 emissions for 2008 by a factor 3.5±0.25 (1σ) (corresponding to 0.59 (0.50-0.67; 2σ) Tg CH_4 yr^{-1}). For validation purpose, we also assume that for our 4C hotspot the correct emissions are 0.59 Tg CH_4 yr^{-1}. This emission estimate is used to 'calibrate' our low-resolution model approach. The difference between the two estimates is used to determine a correction factor to scale the estimates derived from our method, and which will also be used for the estimation of the Chinese target source.

The problem of partially different areas is still present, and this is accounted for an uncertainty change on the correction factor. Note that we use the SCIAMACHY measurements from 2003 to 2009 for consistency with the *Kort et al. (2014)*.

2.3. Target Emission and Area Selection

In a next step, our 'calibrated' emission estimation method is applied to the local source in SS (Figure 6), with a methane hotspot after the elevation correction, and is verified by the latest EDGAR draft v4.3.2. We can see this location is a methane emission hotspot clearly from Figure 6.

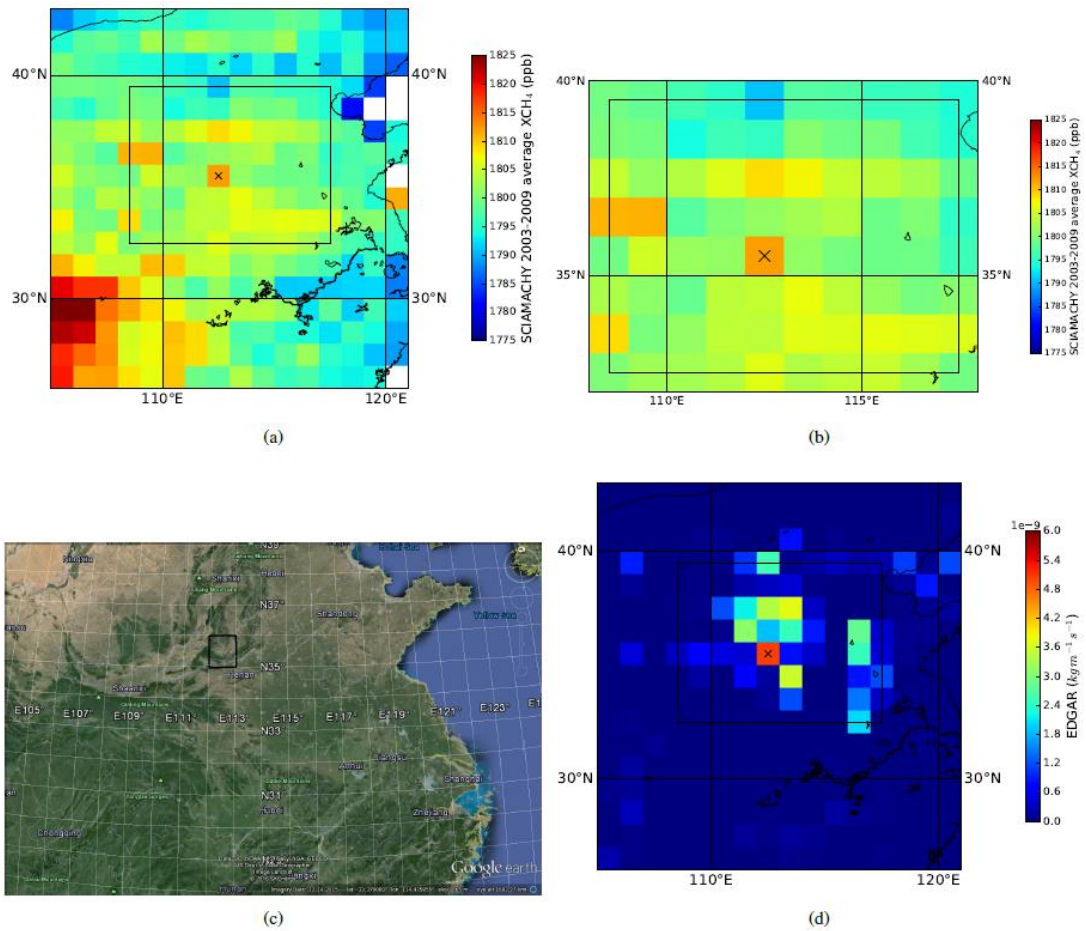

Figure 6. Elevation corrected XCH_4 from SCIAMACHY for the outer-Shānxī source area averaged over 2003-2009 (a and b). (c) shows the outer-Shānxī source area. The EDGAR draft for version v4.3 for the year 2012 containing Gas, Oil, Brown Coal and Hard Coal is shown in d), source: European Commission, Joint Research Centre (JRC)/Netherlands Environmental Assessment Agency (PBL). Emission Database or Global Atmospheric Research (EDGAR), http://edgar.jrc.ec.europe.eu. (from *J. W., 2016*)

3. Results

3.1. Elevation Corrections

In the first step, we choose 25 locations on the earth surface to explore how the elevation correction varies with latitudes, longitudes and time.

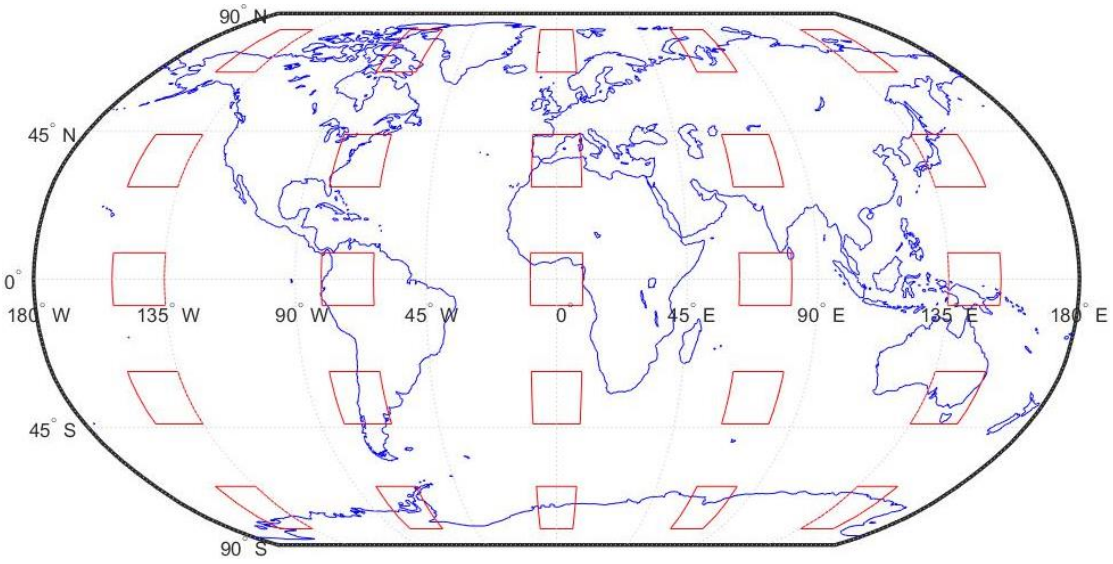

Figure 7. Selected regions for evaluating the global variation in elevation correction using TM5. Every box is lat: 7° × lon: 5°.

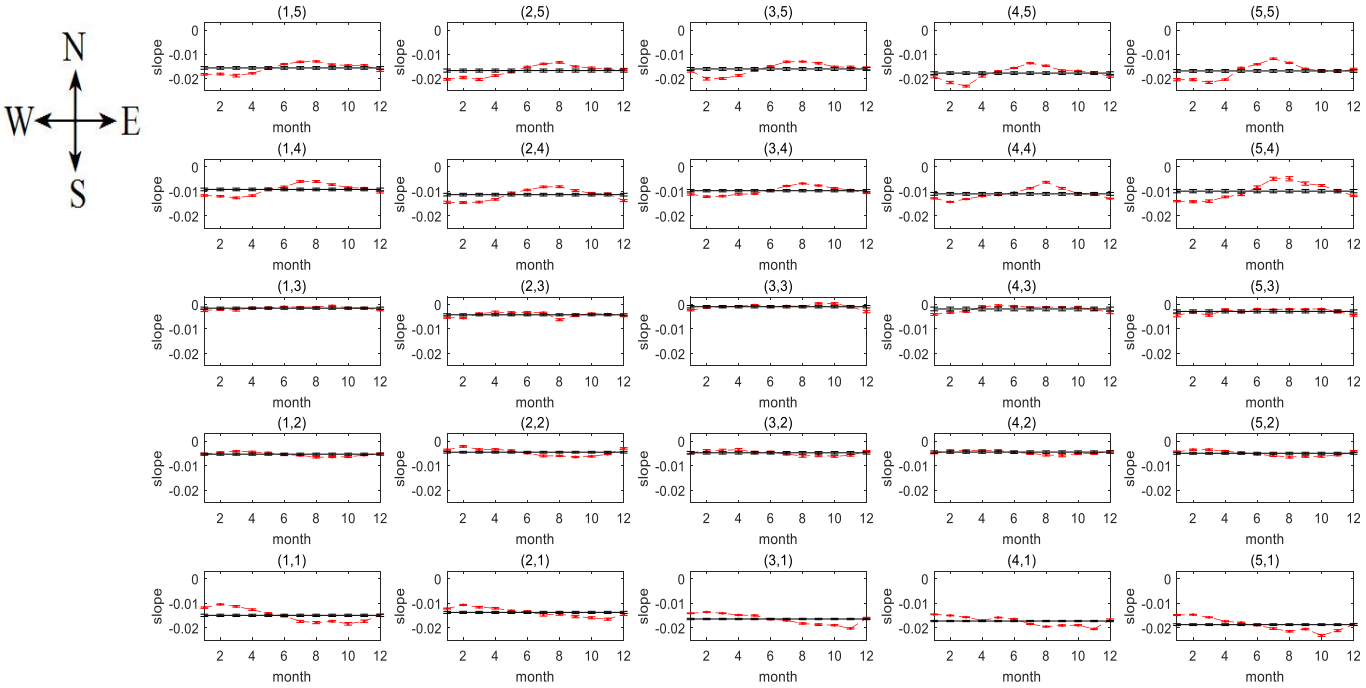

Figure 8. Elevation correction in ppb/m (i.e. the slopes of the regression equation) derived from TM5 for the 25 regions shown in Figure 7. Black line: the annually averaged correction. Red line: the average for each month.

As can be seen in Figure 8, elevation corrections are relatively uniform in zonal direction. However, much larger variations are found in latitudinal direction. At the mid-latitudes of the Northern Hemisphere the largest seasonal variations are found. Overall the variations that are found can be explained by the seasonal dynamics of tropopause height. However, in the Southern Hemisphere the seasonal variation at mid-latitudes is much less clear than in the Northern Hemisphere. It implies the seasonal variation of tropopause height is not the only

factor explaining the variation in elevation correction. In the Southern Hemispheric troposphere, variations in the vertical gradient due to a seasonally varying inflow of methane from the Northern Hemisphere may play a role, too. Based on the information gained from Figure 8, the TM5 model is used to derive a global elevation correction factor matrix as a function of time and latitude (see Figure 9).

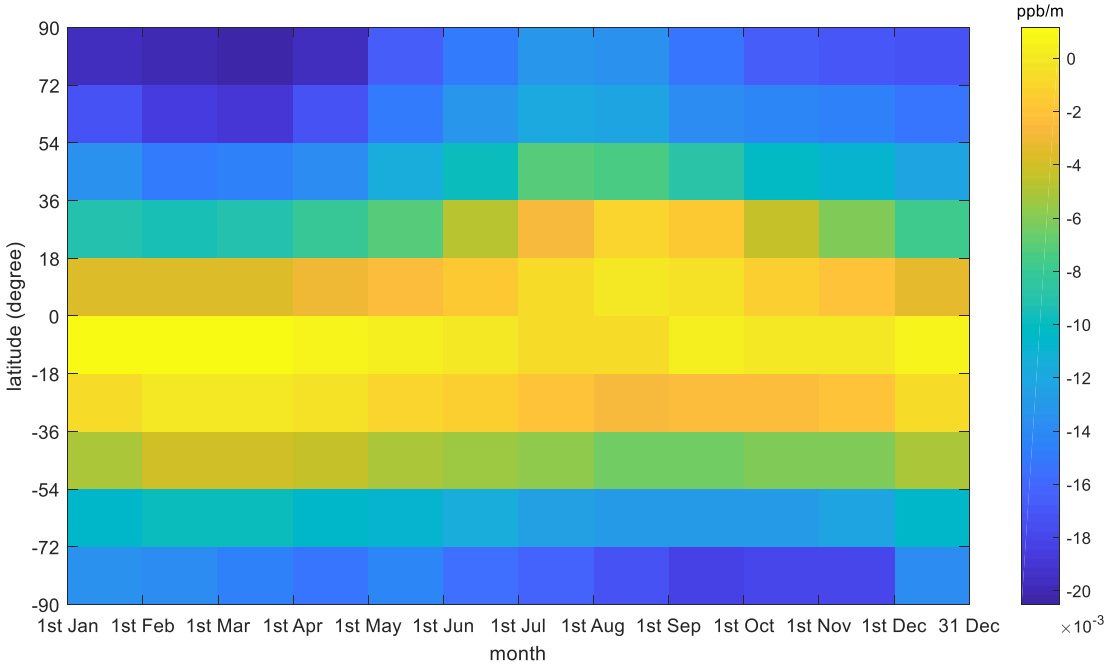

Figure 9. Elevation correction factor matrix for the globe, derived from the TM5 model.

The result in Figure 9 confirms our expectations. First, the elevation correction factor varies with time, with a seasonal amplitude maximizing at the mid latitudes of the Northern Hemisphere. The values are negatively correlated with tropospheric air temperatures. Second, latitudinal variation exists, with smallest corrections in the Tropics. This is expected since this is where the tropopause as highest and the stratospheric sub-column is most shallow. Furthermore, the seasonal variation shifts in phase moving from north to south. These variations are all expected from known variations in tropopause height, changing the ratio of stratosphere and troposphere thicknesses. The interpolated matrix for every single latitude grid is shown in Figure 10.

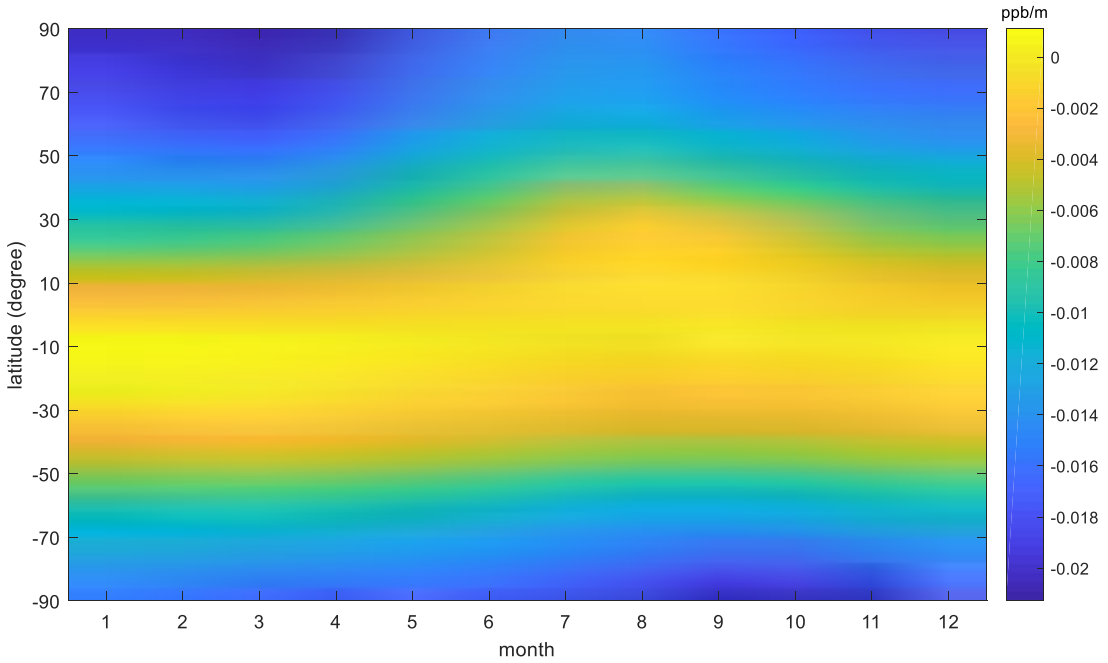

Figure 10. The interpolated global elevation correction matrix from TM5 data.

In the next step, the model derived elevation correction matrix is tested in three regions against regressions derived from the SCIAMACHY data: 4C, Middle East and Sahara (see Figure 11). The motivation for selecting these regions are that the 4C region is has been well studied in the past. The Middle East and Sahara are usually cloud free, and therefore many satellite retrievals are available. In addition, in uninhabited arid regions methane emissions are usually low.

The size selection criteria described in Section 2.2.2 are applied for each region. In the end, we decided to choose 4C small, Middle East large and Sahara small as the most suitable sizes for validation.

Comparing SCIAMACHY and TM5 derived elevation corrections the difference between the two can by plotted in the same manner as in Figure 9 for each of the three regions (see Figure 11).

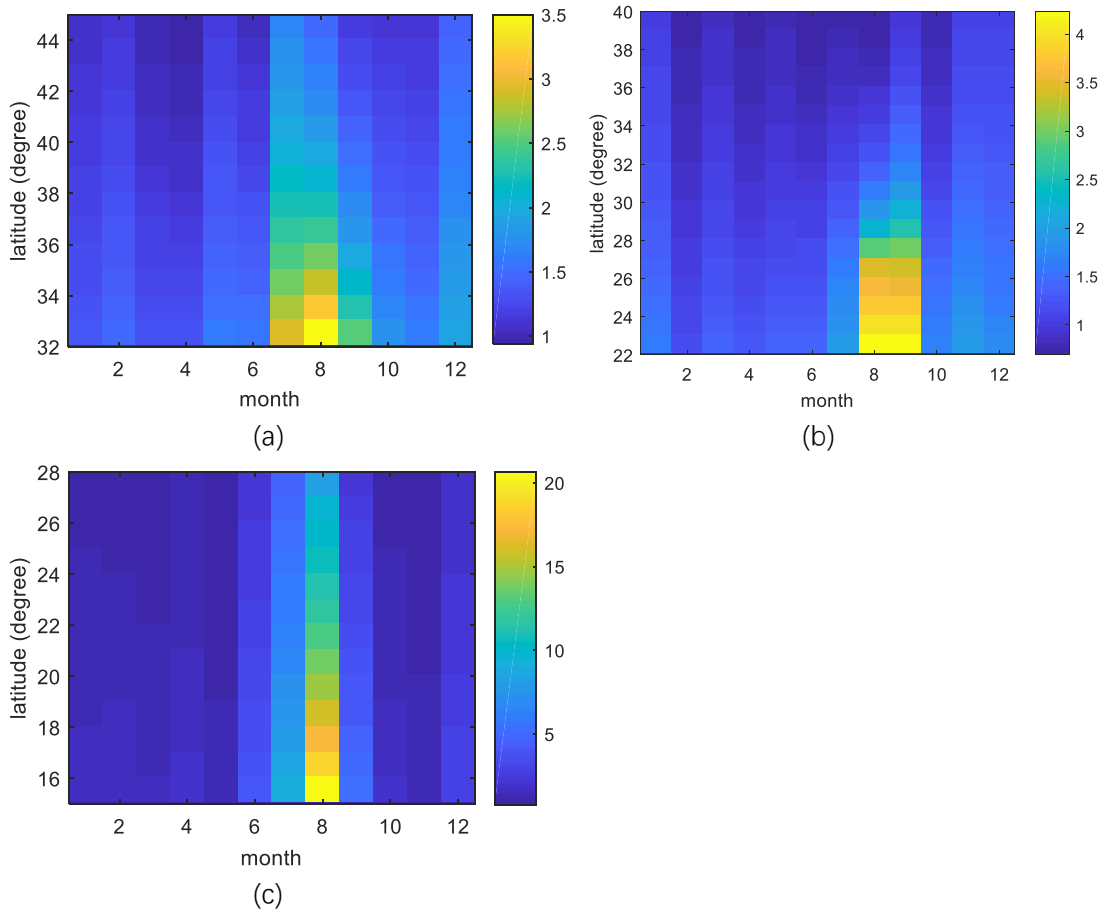

Figure 11. Differences between SCIAMACHY and TM5 derived slopes correction slopes SCIAMACHY/TM5 for (a) 4C, (b) Middle East and (c) the Sahara.

In Figure 11, we see that the elevation corrects from TM5 and SCIAMACHY are quite consistent for 4C and Middle East. However, the Sahara shows differences up to an order of magnitude during summer. This result implies that the elevation dependence of SCIAMACHY XCH_4 is not always explained by the TM5 simulated vertical profile of methane, but may have other influences, for example, the presence of high aerosol loading in desert areas. Aerosol scattering increases the light path in the planetary boundary layer over the desert also, changing the ratio of stratospheric and tropospheric contributions to the total column in a way that is not presented by TM5. For this reason, we decided to exclude the difference between the TM5 and SCIAMACHY derived elevation correction for the Sahara, and only use the other two validation regions to fine tune the elevation correction matrix. From these regions, we derive a factor of 1.37 by which the matrix should be scaled to bring the TM5 derived estimates in agreement with SCIAMACHY. The modified elevation correction matrix is shown below in Figure 12.

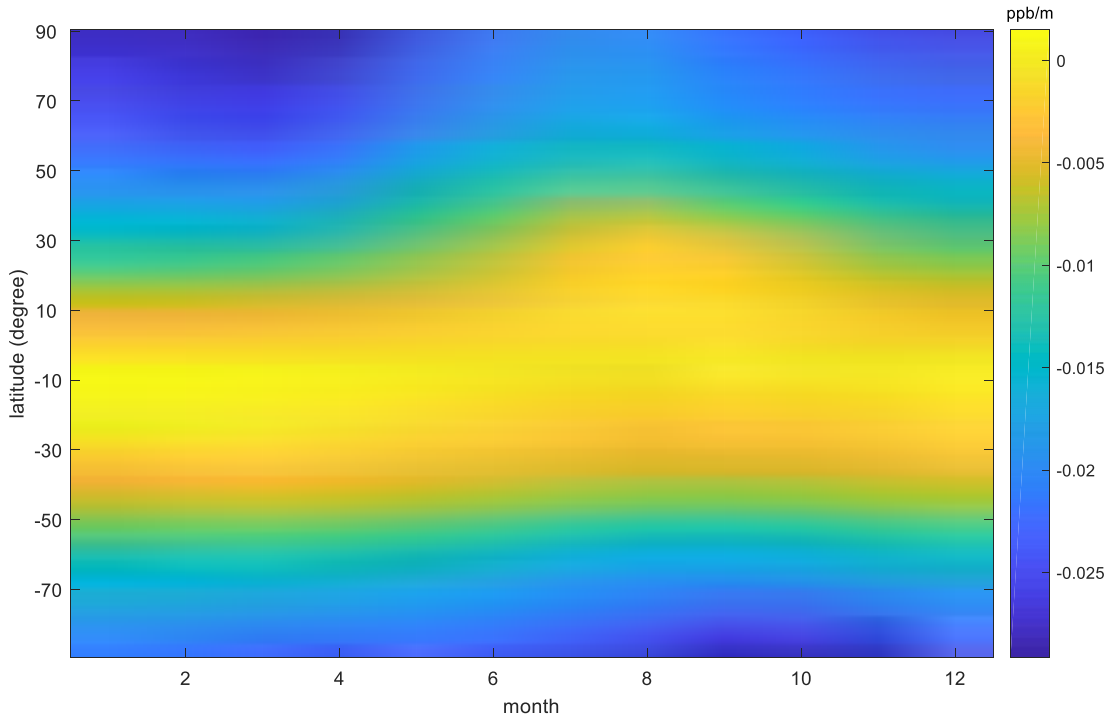

Figure 12. Modified global elevation correction matrix derived from TM5, and improved using SCIAMACHY.

The global elevation correction matrix of Figure 12, can now be used to correct SCIAMACHY data everywhere in the world. This map can be compared with the original SCIAMACHY map to separate orographic influences from emission influences on XCH_4.

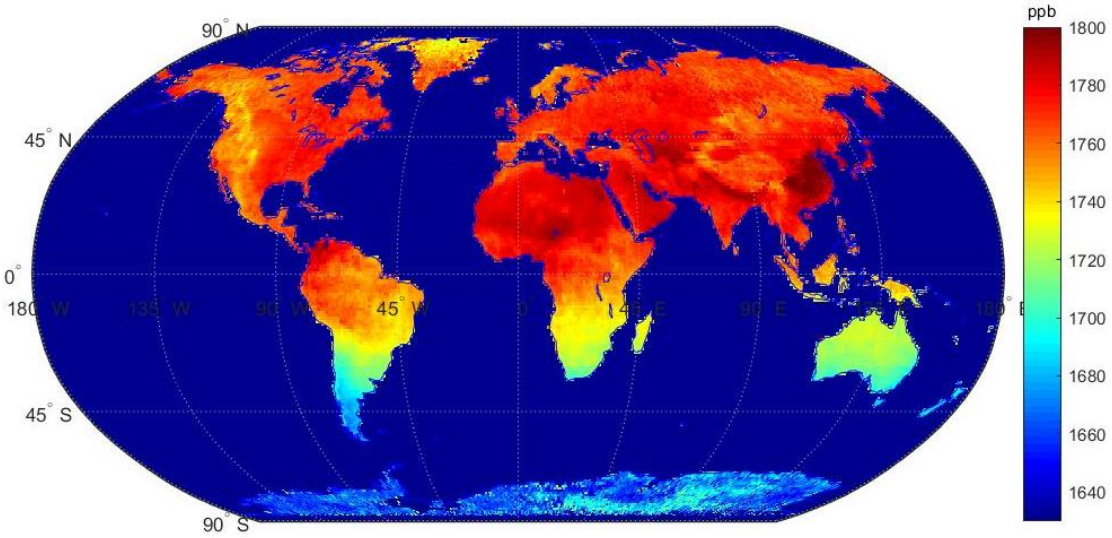
ppb
1800
1780
1760
1740
1720
1700
1680
1660
1640
90° N
45° N
0°
180° W
45° W
45° E
90° E
45° S
90° S

(a)

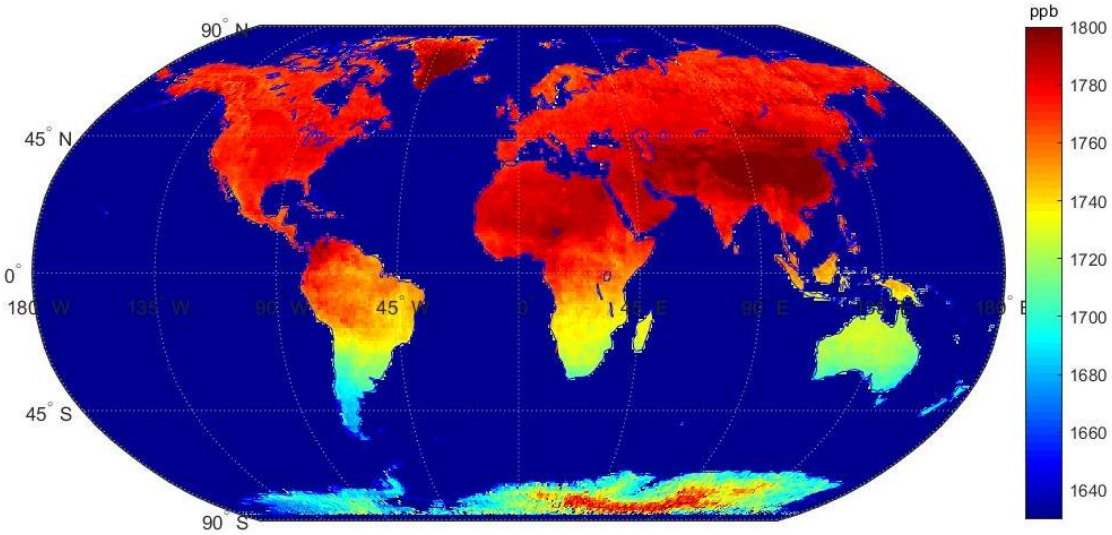
ppb
1800
1780
1760
1740
1720
1700
1680
1660
1640
90° N
45° N
0°
180° W
45° W
45° E
90° E
45° S
90° S

(b)

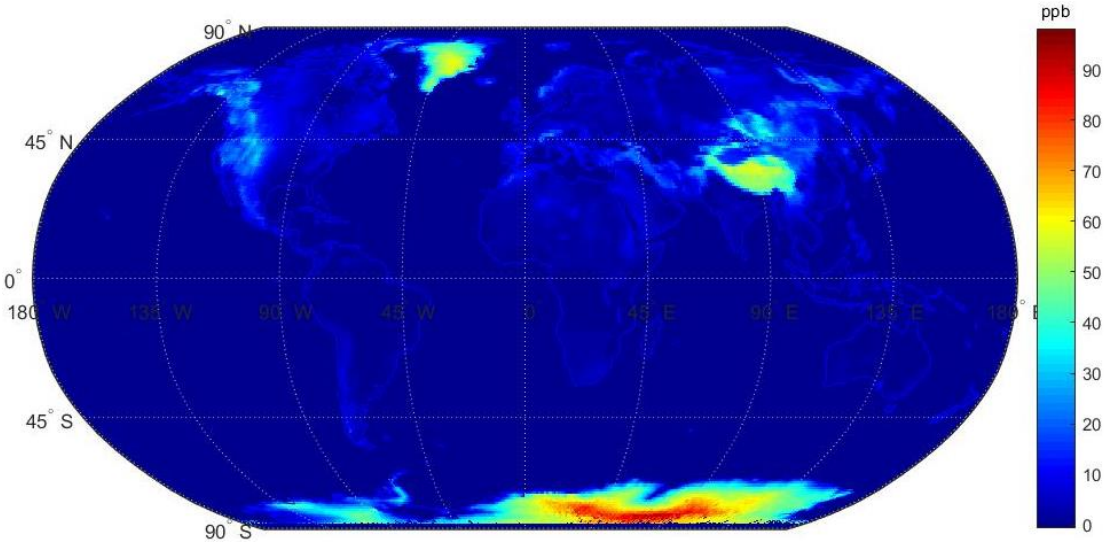
ppb
90
80
70
60
50
40
30
20
10
0
90° N
45° N
0°
180° W
45° W
45° E
90° E
45° S
90° S

(c)

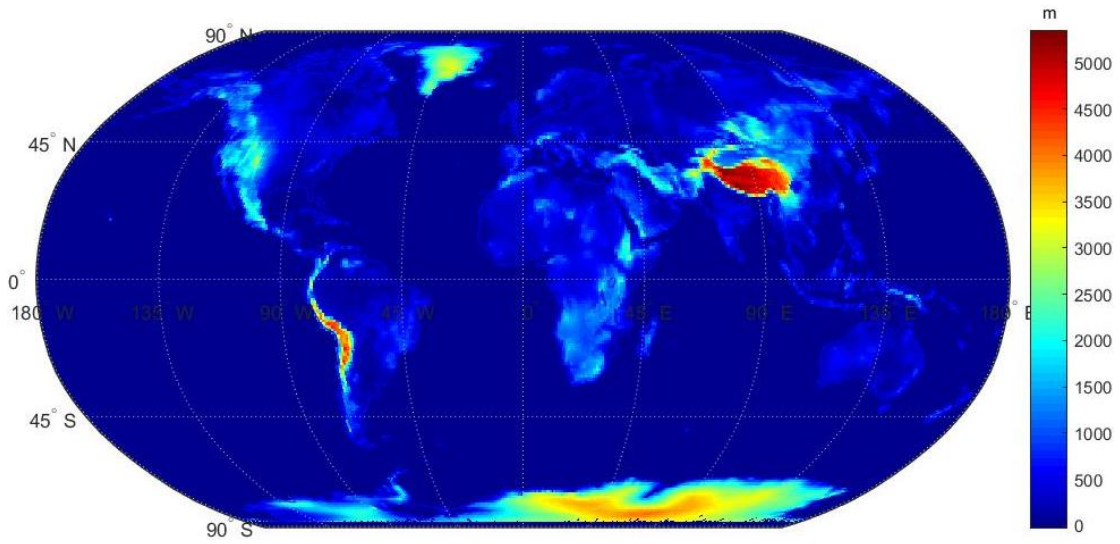

(d)

Figure 13. Global signals of orography in SCIAMACHY XCH_4, comparing (a) the original (uncorrected) global XCH_4 map from SCIAMACHY, (b) the same map after elevation correction with the matrix shown in Figure 12, (c) the difference between (a) and (b), (d) the surface elevation map. All figures are on a 1° × 1° resolution.

As expected from the results in Figure 12 the impact of the elevation correction is small in the Tropics (see Figure 13). In the mid latitudes, the elevation correction matrix has the largest impact, showing clear differences between the two maps, especially in West North America, Middle East and East Asia. Interestingly, the signature of orography in the original dataset largely disappears, as can be seen very clearly over North America. The impact at mid latitudes is largest because of significant mountain ranges in America and Asia. In the regions with high altitude plateaus, for example the Tibetan Plateau, the Antarctic, and Greenland, the elevation correction seems to over correct the elevation signal in the data. This might be due to the linear elevation correction equation used in this research. The high methane mole fractions in those regions are probably overestimated for that reason. However, since we are mainly interested to apply the elevation correction to the CH_4 emission hotspot in SS, the problem at high elevation is not relevant for our purpose.

3.2. Determining Emissions

3.2.1. Four Corners

SCIAMACHY observation

The SCIAMACHY XCH_4 data averaged from 2003 to 2009 is shown at 1° × 1° resolution in Figure 14.

In these figures, the area from the 4C paper (*Kort el al., 2014*) is marked.

The two grid-cells with the highest XCH_4 values are defining the 4C source area.

Elevation corrected SCIAMACHY observation

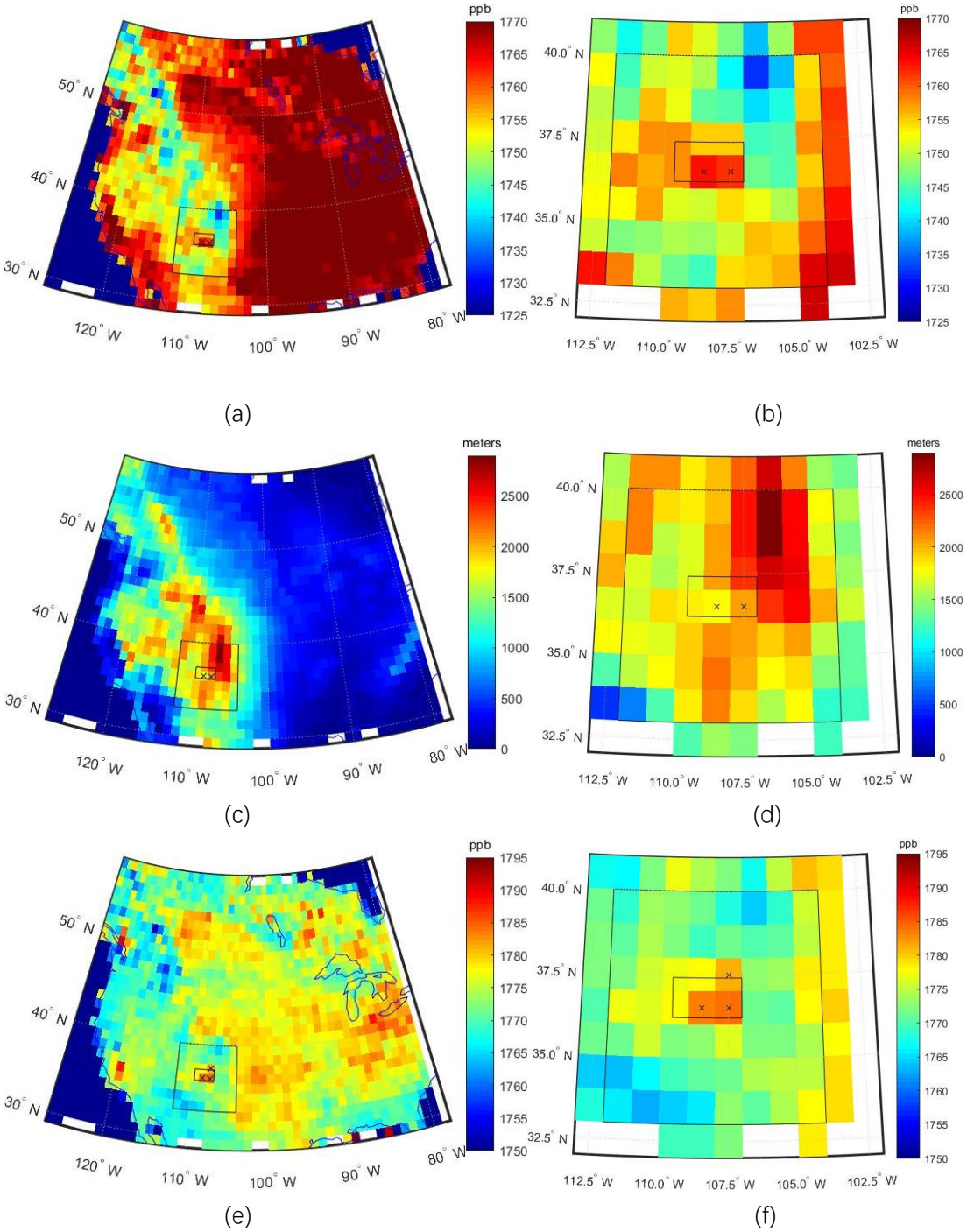

Figure 14. (a), (b) show the gridded SCIAMACHY XCH_4 data map in 4C region; (c), (d) show the surface elevation map; (e), (f) show the elevation corrected XCH_4 map. Resolution: 1°×1°. Time: 2003 to 2009. The black crosses mark 4C source region. The adjusted hotspots are marked in (f).

In Figure 14, after the elevation correction, the color scale of XCH_4 is increased by 25 ppb. This is the effect of elevation correction. The result in Figure 14(f) shows an adjust of the

definition of 4C source region is required, which is already shown on the figure.

ΔXCH_4

20% of all grid cells with the lowest XCH_4 values are chosen for the background analysis, in the small, medium and large sizes respectively. It is shown in Figure 15.

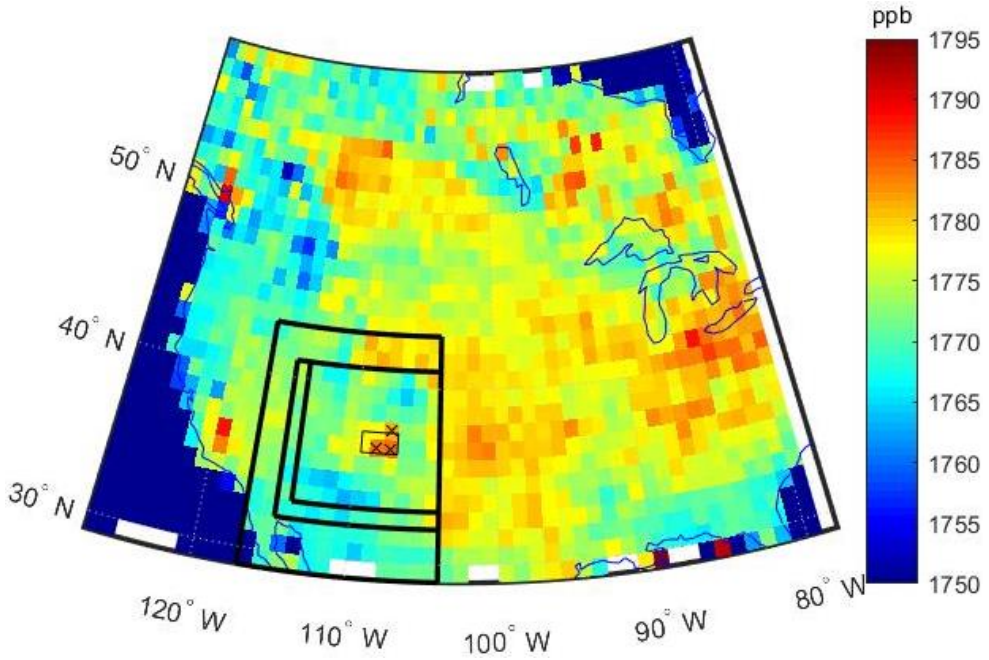

Figure 15. Background analysis of 4C. The three thick black squares represent the small, medium, large sizes for background analysis. 20% of the grid cells inside the squares with lowest XCH_4 values are chosen. The black crosses represent the hotspot region. The thin black square shows the 4C source region defined in *Kort et al., 2014*.

Table 4. Results for 4C source background analysis (unit: ppb).

	XCH_4	1σ uncertainty
Source	1783.56	0.80
Background small	1766.29	0.41
Background medium	1766.34	0.33
Background large	1766.48	0.24
Difference small	17.27	0.90
Difference medium	17.22	0.87
Difference large	17.08	0.84

From Table 4, we can see the XCH_4 values among different sizes vary slightly. So, we choose the one with the smallest uncertainty, which is background large in this case. The ΔXCH_4 is 17.08±0.84 ppb.

ΔEMI

Rewrite Equation 17 to get Equation 19, where ΔEMI_{TM5} is set to be 1 Tg·yr^{-1}.

$$\Delta EMI = \frac{\Delta XCH_4}{\Delta XCH_4\_TM5} \times \Delta EMI_{TM5} = \frac{\Delta XCH_4}{\Delta XCH_4\_TM5} \times 1\ \mathrm{Tg \cdot yr^{-1}}$$

(19)

Now we can determine *ΔEMI*. The modeled plume for a single grid-cell in the 4C region is shown in Table 5.

Table 5. Average XCH_4 on 5×5 grid, output of TM5 forward run for the year 2014, units (ppb), at 1°×1° resolution. The center of the center cell is located at lat 36.5°N and lon -107.5°W. The input is an emission of 1 Tg·yr^{-1} by the center grid-cell and no emission from the surrounding cells.

1.35	1.51	1.41	1.54	1.75
1.60	2.46	3.58	3.77	3.39
1.39	3.52	13.23	8.27	4.26
1.15	1.51	3.80	4.59	3.53
1.04	1.12	1.28	1.94	2.06

Because the hotspot consisted of three grid-cells, the modeled plume had to be extrapolated to the other two grid-cells. For the three source-cells in the 4C region the modeled ΔxCH_4_TM5 values are shown in Table 6.

Table 6. Modeled XCH_4 enhancement in (ppb) of the three grid-cells that form the source-area. The three grid-cells are shown in Figure 15.

-	20.58±2.14
18.26±2.17	25.30±2.31

The average ΔxCH_4_TM5 over these grid-cells is (20.58+18.26+25.30)/3=21.38±1.27ppb. *ΔXCH₄* according to SCIAMACHY is 17.08±0.84 ppb. Now using Equation 19, we find that the *ΔEMI* of each grid-cell in the source area is

$$\frac{17.08}{21.38} \times 1\ \mathrm{Tg \cdot yr^{-1}} = 0.80 \pm 0.06\ \mathrm{Tg \cdot yr^{-1}}$$

There are three source grid cells in the area, thus the *ΔEMI* of the source-area is

$$0.80 \times 3\ \mathrm{Tg \cdot yr^{-1}} = 2.40 \pm 0.18\ \mathrm{Tg \cdot yr^{-1}}$$

EMI

Note that *ΔEMI* is with respect to 4C background large. For *EMI* of the source area a background emission must be added. The average emission of 4C background large is 4.176

$\times 10^{-11}$ kg · m^{-2} · s^{-1} according to EDGAR draft v4.3.2 'total'. The total area of the source area is 29662 km^2. Hence the background emission (*EMI_background*) of the 4C source area is 0.039 Tg · yr^{-1}. Note that this background emission is only 1.6% of *ΔEMI*. The *EMI* of the source area is therefore 2.44±0.18 Tg · yr^{-1}.

Validation to Four Corners hotspot

As is described in subsection 2.2.5, a validation is performed using the 4C hotspot. For validation purpose, we assume here that for our 4C hotspot, the correct emissions are 3.5 times the EDGAR emissions v4.2 'Total'.

From the 4C article (*Kort et al., 2014*), this factor 3.5±0.25 (1σ) is obtained. However, the error on this factor is underestimated because of the different EDGAR version in this research, and partially different areas. Therefore, corrections on this factor for this research must be applied.

In 'EDGAR draft v4.3.2 2008 total', the emission for the source area defined in *Kort et al. (2014)* (-109.6°W to -107.0°W and 36.2°N to 37.4°N) is 6.24×10^{-11} kg · m^{-2} · s^{-1}, hence the total emission is 0.061 Tg · yr^{-1}. However in the paper, the inventory used is 'EDGAR v4.2 2008 total', with a result of 0.168 Tg · yr^{-1} in the source area. The validation factor derived in *Kort et al. (2014)* is 3.5±0.25 (1σ). The concluded methane emission is 0.59 Tg · yr^{-1} (0.55~0.63; 1σ). This emission is assumed to change little both spatially and in magnitude from year to year. So, the validation factor should be changed to 9.64±0.67 (1σ).

Furthermore, to obtain a more realistic error, the effect of taking different areas must be considered. A pragmatic approach is taken by increasing the error by ratio of hotspot-area outside Kort's area vs source-area inside the Kort's area.

The increase of the error will be calculated first. The total surface area of the source area is 29662 km^2. The area that falls outside the 4C-paper area is 9866 km^2. Hence the ratio of outside vs area inside is 9866/29662=0.33=33%. Therefore, the error is increased by 33% of 9.64. 33% of 9.64 is 3.18. So, the new error on the factor is 0.67+3.18=3.85. Hence for the validation of our methods, we assume that the 'correct emission' for the 4C hotspot is 9.64± 3.85 times the 'EDGAR draft v4.3.2 2008 total'.

The average 'EDGAR draft v4.3.2 2008 total' emission of our source-area is 6.39×10^{-11} kg · m^{-2} · s^{-1}. Hence the total emission according to EDGAR is 0.060 Tg · yr^{-1}. So, our emission is 2.44/0.060=40.67 ± 3.00 times the EDGAR emission. This should have been 9.64 ± 3.85 according to validation, hence the overestimate of our emission method is 40.67/9.64=4.22± 1.71.

This factor 4.22±1.71 is the correction factor that is applied to the other hotspots.

Applying this correction factor to the 4C hotspot gives *EMI*=2.44/4.22=0.58±0.24 Tg · yr^{-1} (which is 9.64 times EDGAR emission of 0.060 Tg · yr^{-1}).

Comparison to EDGAR

EDGAR draft v4.3.2 2008 total of methane emission is shown in Figure 16. It is clearly seen that 4C is a hotspot according to EDGAR.

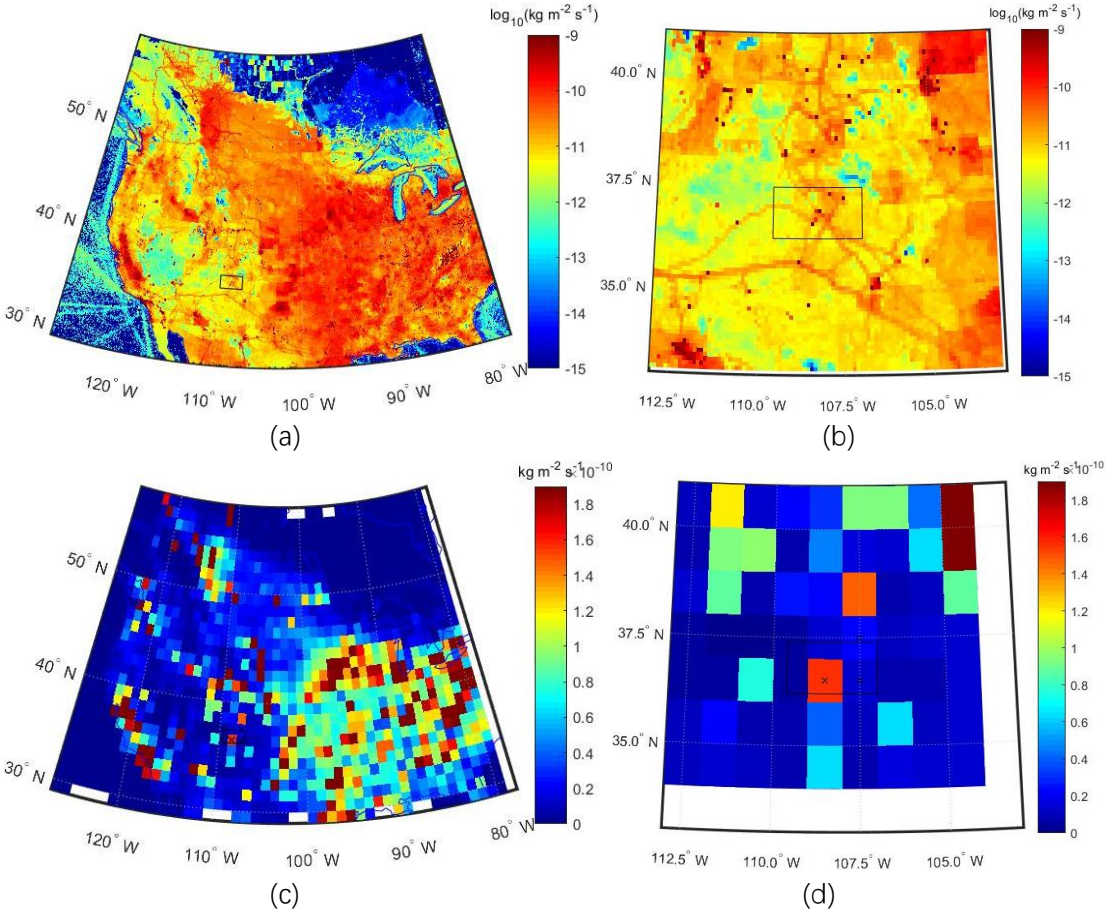

Figure 16. EDGAR draft v4.3.2 total CH_4 emission for 4C in 2008. Resolution: (a), (b): 0.1° ×0.1°, (c), (d): 1°×1°

Table 7. EDGAR draft v4.3.2 CH_4 emissions from the 4C source area, and the source area + surrounding grid-cells.

4C	Surrounding	Source	Surrounding	Source
Area (km^2)	148049	29662		
EDGAR category	Avg ($kg \cdot m^{-2} \cdot s^{-1}$)	Avg ($kg \cdot m^{-2} \cdot s^{-1}$)	Total ($Tg \cdot yr^{-1}$)	Total ($Tg \cdot yr^{-1}$)
Agricultural soils	0	0	0	0
Agricultural waste burning	4.29×10^{-15}	6.52×10^{-16}	2.01×10^{-5}	6.12×10^{-7}
Production of chemicals	1.64×10^{-14}	2.00×10^{-15}	7.70×10^{-5}	1.87×10^{-6}
Energy industry	1.19×10^{-13}	5.44×10^{-13}	5.58×10^{-4}	5.10×10^{-4}
Enteric fermentation	5.90×10^{-12}	4.73×10^{-12}	2.76×10^{-2}	4.44×10^{-3}
Fossil fuel fires	8.06×10^{-13}	4.03×10^{-12}	3.77×10^{-3}	3.78×10^{-3}
Manufacturing Industry	2.26×10^{-14}	2.69×10^{-15}	1.06×10^{-4}	2.52×10^{-6}
Production of iron and steel	0	0	0	0
Large scale biomass burning	1.22×10^{-14}	1.38×10^{-14}	5.72×10^{-5}	1.30×10^{-5}
Manure management	5.99×10^{-13}	4.80×10^{-13}	2.81×10^{-3}	4.50×10^{-4}
Fuel combustion and production	2.37×10^{-11}	5.35×10^{-11}	1.11×10^{-1}	5.02×10^{-2}
Residential	1.98×10^{-13}	1.35×10^{-13}	9.27×10^{-4}	1.26×10^{-4}
Oil refineries, transformation industry	2.42×10^{-14}	4.26×10^{-14}	1.13×10^{-4}	3.99×10^{-5}
Solid waste disposal	3.07×10^{-12}	1.83×10^{-14}	1.44×10^{-2}	1.72×10^{-5}
Non-road transport	6.85×10^{-15}	5.54×10^{-15}	3.21×10^{-5}	5.20×10^{-6}
Road transport	2.33×10^{-13}	2.61×10^{-13}	1.09×10^{-3}	2.45×10^{-4}
Waste water	6.40×10^{-13}	1.93×10^{-13}	3.00×10^{-3}	1.81×10^{-4}
Total	3.54×10^{-11}	6.39×10^{-11}	1.66×10^{-1}	6.00×10^{-2}
Our source emission ($Tg \cdot yr^{-1}$)			0.58±0.24	

3.2.2. South Shānxī

The hotspot is called South Shānxī (SS) is because it lies in the south of Shānxī Province, China. The area is shown in Figure 6. Now we are going to do the emission estimation again with the new method we develop in this research.

SCIAMACHY observation

The SCIAMACHY XCH_4 data averaged from 2003 to 2009 is shown at $1° \times 1°$ resolution in Figure 17. The grid-cell with the highest XCH_4 value is defining the SS source area.

Elevation corrected SCIAMACHY observation

The elevation corrected SS region is shown in Figure 17.

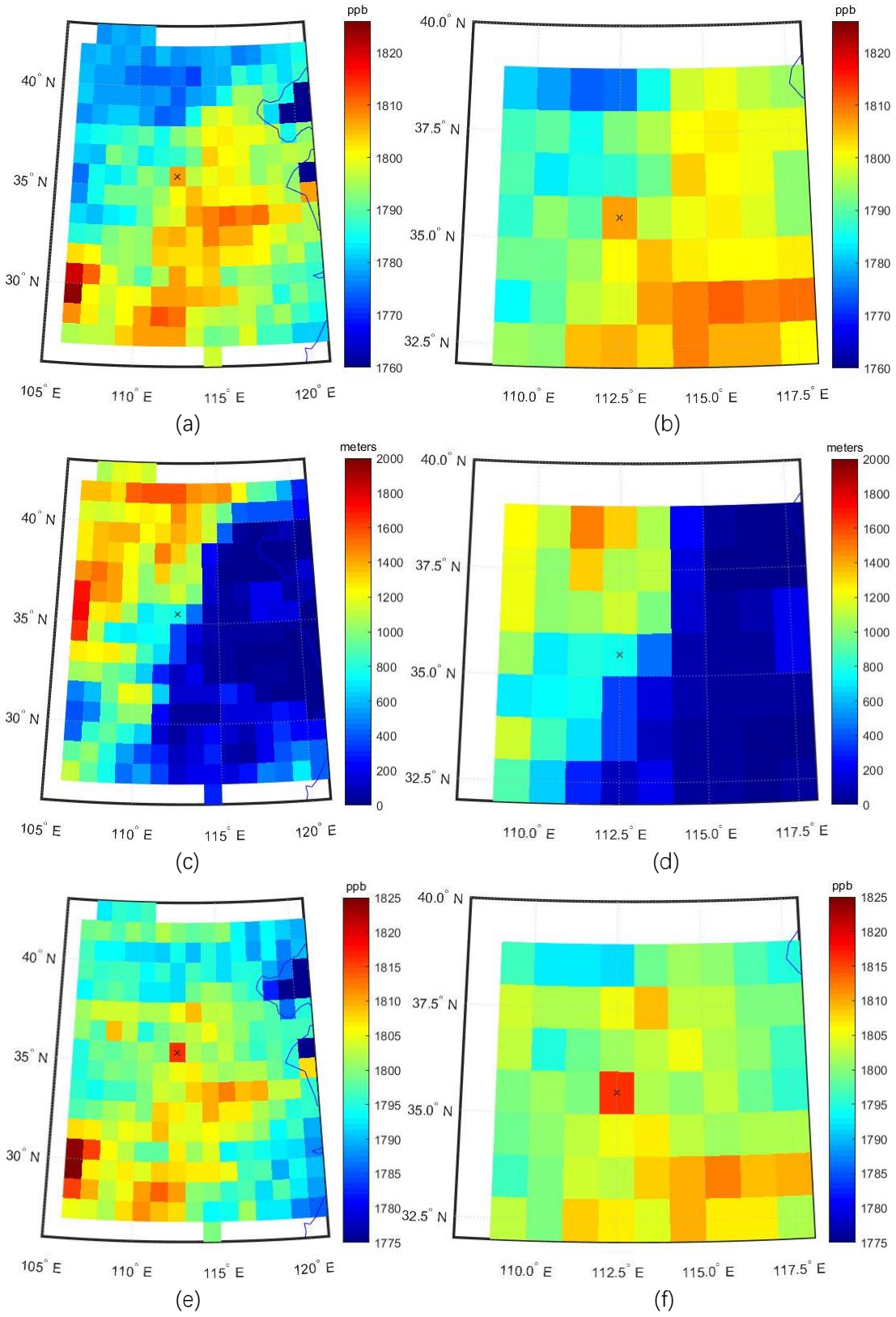

Figure 17. SS region at 1°×1°. (a) and (b) show the SCIAMACHY XCH_4 data averaged from 2003 to 2009. (c) and (d) show the average ground pixel elevation. (e) and (f) show the SCIAMACHY XCH_4 data averaged from 2003 to 2009 after the elevation correction. The black cross marks the SS source area.

ΔXCH_4

20% of all grid cells with the lowest XCH_4 values are chosen for the background analysis, in the small, medium and large sizes respectively. It is shown in Figure 18.

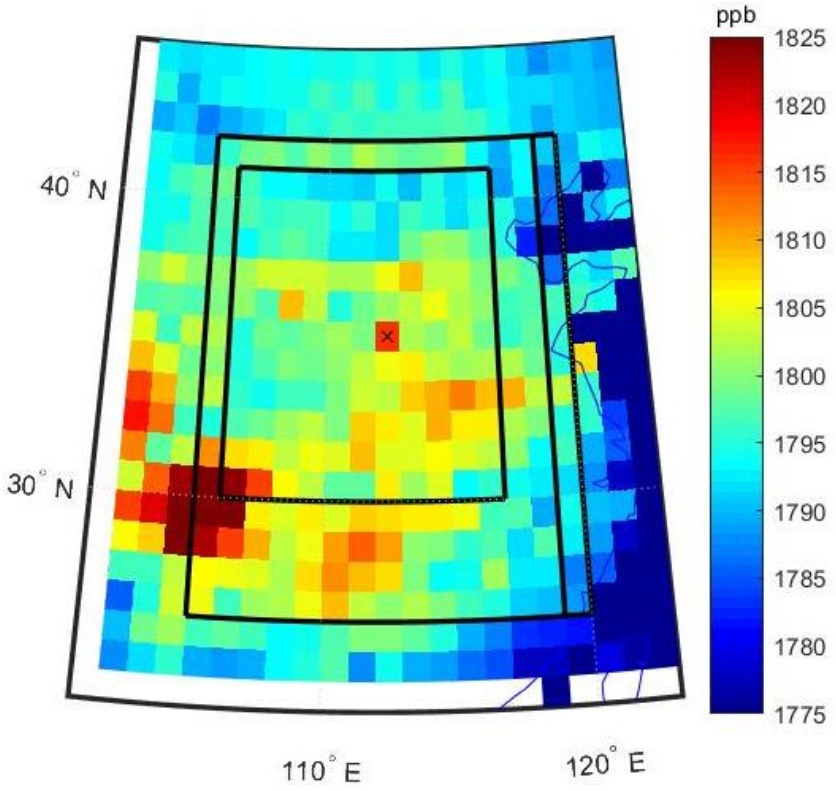

Figure 18. Background analysis of SS. The three thick black squares represent the small, medium, large sizes for background analysis. 20% of the grid cells inside the squares with lowest XCH_4 values are chosen. The black cross represents the hotspot region.

Table 8. Results for SS source background analysis (unit: ppb).

	XCH_4	1σ uncertainty
Source	1815.90	1.69
Background small	1793.10	0.26
Background medium	1792.80	0.21
Background large	1792.34	0.21
Difference small	22.80	1.71
Difference medium	23.10	1.70
Difference large	23.56	1.70

From Table 8, we can see the XCH_4 values among different sizes vary slightly. So, we choose the one with the smallest uncertainty, which is background large in this case. The ΔXCH_4 is 23.56±1.70 ppb.

ΔEMI

The modeled plume for a single grid cell in the SS region is shown in Table 9.

Table 9. Average XCH_4 on 5×5 grid, output of TM5 forward run for the year 2014, units (ppb), at 1°×1° resolution. The center of the center cell is located at lat 35.5°N and lon 112.5°E. The input is an emission of 1 $Tg \cdot yr^{-1}$ by the center grid-cell and no emission from the surrounding cells.

1.59	1.89	2.08	2.34	1.97
1.91	2.73	4.59	4.08	2.69
2.36	5.67	13.90	6.76	3.34
2.45	4.26	5.50	4.15	3.35
2.08	2.54	2.51	2.60	2.64

ΔXCH_4 for an emission of 1 $Tg \cdot yr^{-1}$ for the SS hotspot according to the model is 13.90±1.50 ppb. ΔXCH_4 according to SCIAMACHY is 23.56±1.70 ppb. Therefore ΔEMI of the source grid cell in the source area is 23.56/13.90=1.69±0.22 $Tg \cdot yr^{-1}$.

EMI

Note that ΔEMI is with respect to SS background large. For EMI of the source area a background emission must be added. The average emission of SS background large is 3.51×10^{-10} $kg \cdot m^{-2} \cdot s^{-1}$ according to EDGAR draft v4.3.2 'total'. The total area of the source area is 10067 km^2. Hence the background emission (*EMI_background*) of the 4C source area is 0.112 $Tg \cdot yr^{-1}$. Note that this background emission is only 6.6% of ΔEMI. The EMI of the source area is therefore 1.80±0.22 $Tg \cdot yr^{-1}$.

Applying the correction factor

In subsection 3.2.1, it is determined that the emissions are over-estimated by a factor of 4.22 ±1.71. Applying this correction factor to SS, we get an emission rate of 1.80/4.22=0.43±0.18 $Tg \cdot yr^{-1}$.

Comparison to EDGAR

EDGAR draft v4.3.2 'total' is shown in Figure 19.

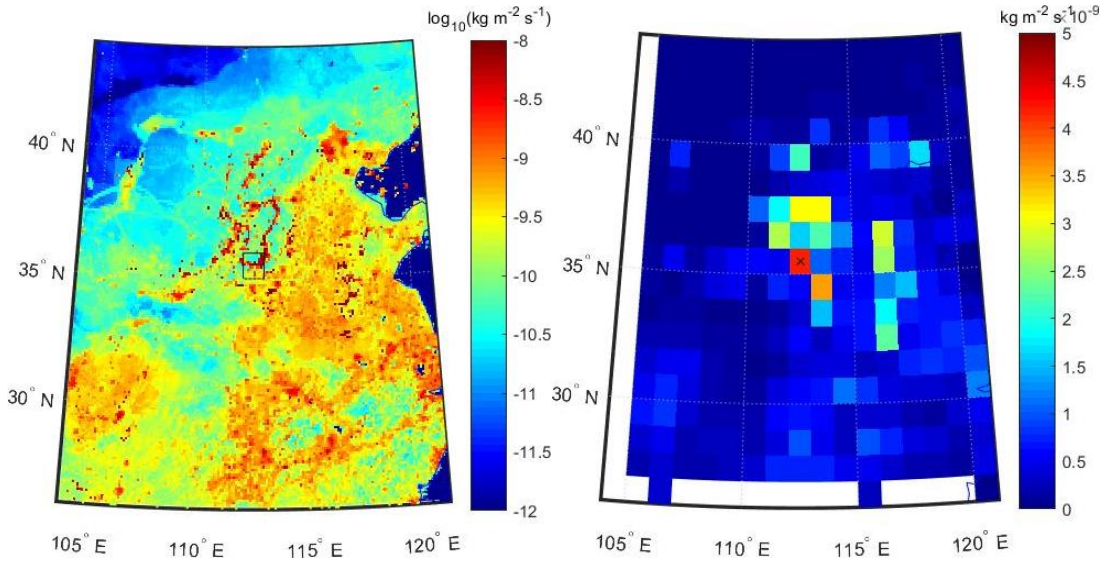

(a) (b)

Figure 19. EDGAR draft v4.3.2 total CH_4 emission for SS in 2008. Resolution: (a): 0.1°× 0.1°, (b): 1°×1°

The tabulated information for SS source and SS source + immediate surrounding is shown in Table 10. It shows the highest and dominant source sector is hard coal. However, the difference of emission estimations between EDGAR and our method is significant, around 1.61/0.58=2.78 times. It might be because of the coarse resolution, or the inaccuracy of EDGAR inventory, or the insufficiency of elevation correction on SCIAMACHY data.

Table 10. EDGAR draft v4.3.2 CH_4 emissions from the SS source area, and the source area + surrounding grid-cells.

SS	Surrounding	Source	Surrounding	Source
Area (km^2)	90579	10067		
EDGAR category	Avg ($kg \cdot m^{-2} \cdot s^{-1}$)	Avg ($kg \cdot m^{-2} \cdot s^{-1}$)	Total ($Tg \cdot yr^{-1}$)	Total ($Tg \cdot yr^{-1}$)
Agricultural soils	9.77×10^{-12}	1.31×10^{-12}	0.0280	0.000418
Agricultural waste burning	1.26×10^{-13}	8.89×10^{-14}	0.000361	2.83×10^{-5}
Production of chemicals	8.07×10^{-13}	3.55×10^{-13}	0.00231	0.000113
Energy industry	5.64×10^{-13}	8.59×10^{-13}	0.00161	0.000274
Enteric fermentation	7.28×10^{-11}	5.23×10^{-11}	0.208	0.0167
Fossil fuel fires	1.10×10^{-12}	1.65×10^{-12}	0.00316	0.000525
Manufacturing Industry	1.47×10^{-12}	1.08×10^{-12}	0.00420	0.000345
Production of iron and steel	4.33×10^{-14}	0	0.000124	0
Large scale biomass burning	1.45×10^{-14}	5.38×10^{-15}	4.17×10^{-5}	1.71×10^{-6}
Manure management	1.21×10^{-11}	7.70×10^{-12}	0.0347	0.00245
Fuel combustion and production	1.64×10^{-9}	4.03×10^{-9}	4.71	1.28
Residential	4.73×10^{-11}	3.33×10^{-11}	0.136	0.0106
Oil refineries, transformation industry	1.28×10^{-12}	1.06×10^{-13}	0.00368	3.38×10^{-5}
Solid waste disposal	3.10×10^{-11}	1.36×10^{-11}	0.0889	0.00433
Non-road transport	2.95×10^{-14}	1.01×10^{-14}	8.45×10^{-5}	3.20×10^{-6}
Road transport	6.91×10^{-13}	3.84×10^{-13}	0.00198	0.000122
Waste water	8.04×10^{-11}	4.89×10^{-11}	0.230	0.0156
Total	1.90×10^{-9}	4.19×10^{-9}	5.45	1.33
Our source emission ($Tg \cdot yr^{-1}$)			0.43±0.18	

3.2.3. Regridded Four Corners

SCIAMACHY observation

The SCIAMACHY XCH_4 data averaged from 2003 to 2009 is shown at $1° \times 1°$ resolution in Figure 20.
In these figures, the area from the 4C paper (*Kort el al., 2014*) is marked.
The two grid-cells with the highest XCH_4 values are defining the 4C source area.

Elevation corrected SCIAMACHY observation

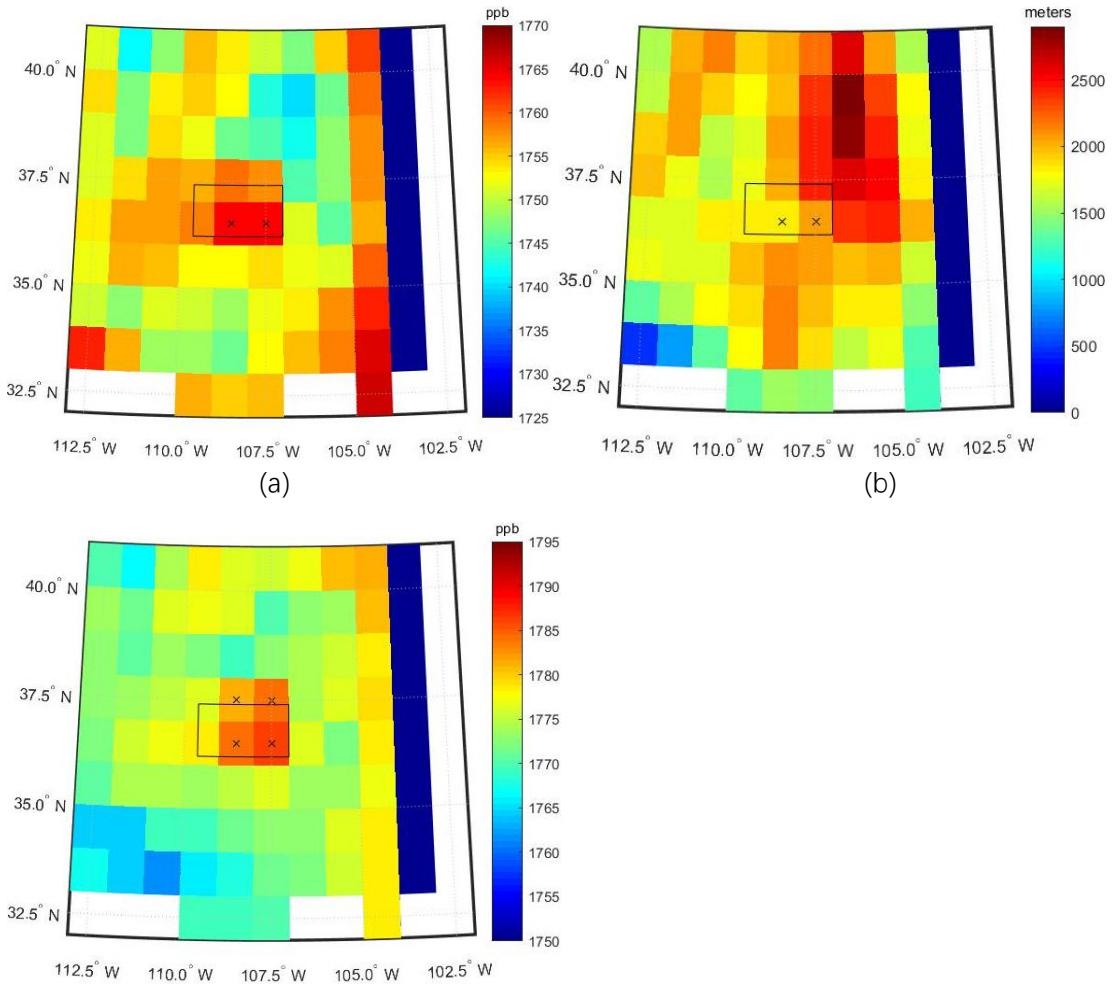

Figure 20. (a) shows the gridded SCIAMACHY XCH_4 data map in 4C region; (b) shows the surface elevation map; (c) shows the elevation corrected XCH_4 map. Resolution: 1°×1°. Time: 2003 to 2009. The black crosses mark 4C source region. The adjusted hotspots are marked in (c).

In Figure 20, after the elevation correction, the color scale of XCH_4 is increased by 25 ppb.

This is the effect of elevation correction. The result in Figure 20(c) shows an adjust of the definition of 4C source region is required, which is already shown on the figure.

ΔXCH_4

20% of all grid cells with the lowest XCH_4 values are chosen for the background analysis, in the small, medium and large sizes respectively. It is shown in Figure 21.

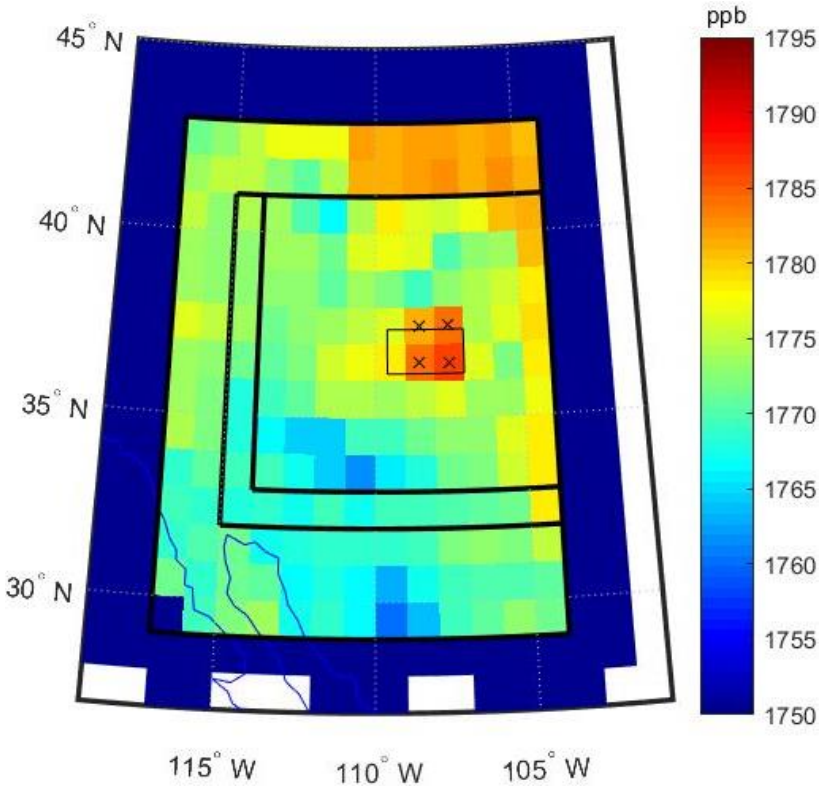

Figure 21. Background analysis of 4C. The three thick black squares represent the small, medium, large sizes for background analysis. 20% of the grid cells inside the squares with lowest XCH_4 values are chosen. The black crosses represent the hotspot region. The thin black square shows the 4C source region defined in *Kort et al., 2014*.

Table 11. Results for 4C source background analysis (unit: ppb).

	XCH_4	1σ uncertainty
Source	1783.80	1.18
Background small	1767.68	0.59
Background medium	1767.47	0.51
Background large	1767.22	0.37
Difference small	16.12	1.32
Difference medium	16.33	1.29
Difference large	16.58	1.24

From Table 11, we can see the XCH_4 values among different sizes vary slightly. So, we choose

the one with the smallest uncertainty, which is background large in this case. The ΔXCH_4 is 16.58±1.24 ppb.

ΔEMI

The modeled plume for a single grid-cell in the 4C region is shown in Table 12.

Table 12. Average XCH_4 on 5×5 grid, output of TM5 forward run for the year 2014, units (ppb), at 1°×1° resolution. The center of the center cell is located at lat 36.5°N and lon -107.5°W. The input is an emission of 1 Tg·yr^{-1} by the center grid-cell and no emission from the surrounding cells.

1.35	1.51	1.41	1.54	1.75
1.60	2.46	3.58	3.77	3.39
1.39	3.52	13.23	8.27	4.26
1.15	1.51	3.80	4.59	3.53
1.04	1.12	1.28	1.94	2.06

Because the hotspot consisted of four grid-cells, the modeled plume had to be extrapolated to the other three grid-cells. For the three source-cells in the 4C region the modeled ΔxCH_4_TM5 values are shown in Table 13.

Table 13. Modeled XCH_4 enhancement in (ppb) of the four grid-cells that form the source-area. The four grid-cells are shown in Figure 21.

22.79±2.27	28.85±2.51
22.06±2.53	29.89±2.69

The average ΔxCH_4_TM5 over these grid-cells is (22.79+28.85+22.06+28.89)/4=25.65 ± 1.25ppb. ΔXCH_4 according to SCIAMACHY is 16.58±1.24 ppb. Now using Equation 19, we find that the *ΔEMI* of each grid-cell in the source area is

$$\frac{16.58}{25.65} \times 1\ \mathrm{Tg \cdot yr^{-1}} = 0.65 \pm 0.06\ \mathrm{Tg \cdot yr^{-1}}$$

There are four source grid cells in the area, thus the *ΔEMI* of the source-area is

$$0.65 \times 4\ \mathrm{Tg \cdot yr^{-1}} = 2.60 \pm 0.24\ \mathrm{Tg \cdot yr^{-1}}$$

EMI

Note that *ΔEMI* is with respect to 4C background large. For *EMI* of the source area a background emission must be added. The average emission of 4C background large is 3.29× 10^{-11} kg·m^{-2}·s^{-1} according to EDGAR draft v4.3.2 'total'. The total area of the source area is 39549 km^2. Hence the background emission (*EMI_background*) of the 4C source area is 0.040 Tg·yr^{-1}. Note that this background emission is only 1.6% of *ΔEMI*. The *EMI* of the source area is therefore 2.64±0.24 Tg·yr^{-1}.

Validation to Four Corners hotspot

As is described in subsection 2.2.5, a validation is performed using the 4C hotspot. For validation purpose, we assume here that for our 4C hotspot, the correct emissions are 3.5 times the EDGAR emissions v4.2 'Total'.

From the 4C article (*Kort et al., 2014*), this factor 3.5±0.25 (1σ) is obtained. However, the error on this factor is underestimated because of the different EDGAR version in this research, and partially different areas. Therefore, corrections on this factor for this research must be applied.

In 'EDGAR draft v4.3.2 2008 total', the emission for the source area defined in *Kort et al., 2014* (-109.6°W to -107.0°W and 36.2°N to 37.4°N) is 6.24×10^{-11} kg · m^{-2} · s^{-1}, hence the total emission is 0.061 Tg · yr^{-1}. However in the paper, the inventory used is 'EDGAR v4.2 2008 total', with a result of 0.168 Tg · yr^{-1} in the source area. The validation factor derived in *Kort et al. (2014)* is 3.5±0.25 (1σ). The concluded methane emission is 0.59 Tg · yr^{-1} (0.55~0.63; 1σ). This emission is assumed to change little both spatially and in magnitude from year to year. So, the validation factor should be changed to 9.64±0.67 (1σ).

Furthermore, to obtain a more realistic error, the effect of taking different areas must be considered. A pragmatic approach is taken by increasing the error by ratio of hotspot-area outside Kort's area vs source-area inside the Kort's area.

The increase of the error will be calculated first. The total surface area of the source area is 39549 km^2. The area that falls outside the 4C-paper area is 15820 km^2. Hence the ratio of outside vs total area is 15820/39549=0.40=40%. Therefore, the error is increased by 40% of 9.64. 40% of 9.64 is 3.86. So, the new error on the factor is 0.67+3.86=4.53. Hence for the validation of our methods, we assume that the 'correct emission' for the 4C hotspot is 9.64± 4.53 times the 'EDGAR draft v4.3.2 2008 total'.

The average 'EDGAR draft v4.3.2 2008 total' emission of our source-area is 5.106×10^{-11} kg · m^{-2} · s^{-1}. Hence the total emission according to EDGAR is 0.064 Tg · yr^{-1}. So, our emission is 2.64/0.064=41.25 ± 3.75 times the EDGAR emission. This should have been 9.64±4.53 according to validation, hence the overestimate of our emission method is 41.25/9.64=4.28± 2.05.

This factor 4.28±2.05 is the correction factor that is applied to the other hotspots.

Applying this correction factor to the 4C hotspot gives *EMI*=2.64/4.28=0.62±0.30 Tg · yr^{-1} (which is 9.64 times EDGAR emission of 0.064 Tg · yr^{-1}).

Comparison to EDGAR

EDGAR draft v4.3.2 2008 'total' of methane emission is shown in Figure 22. It is clearly seen that 4C is a hotspot according to EDGAR. However, the new added left top grid cell is not a hotspot according to EDGAR.

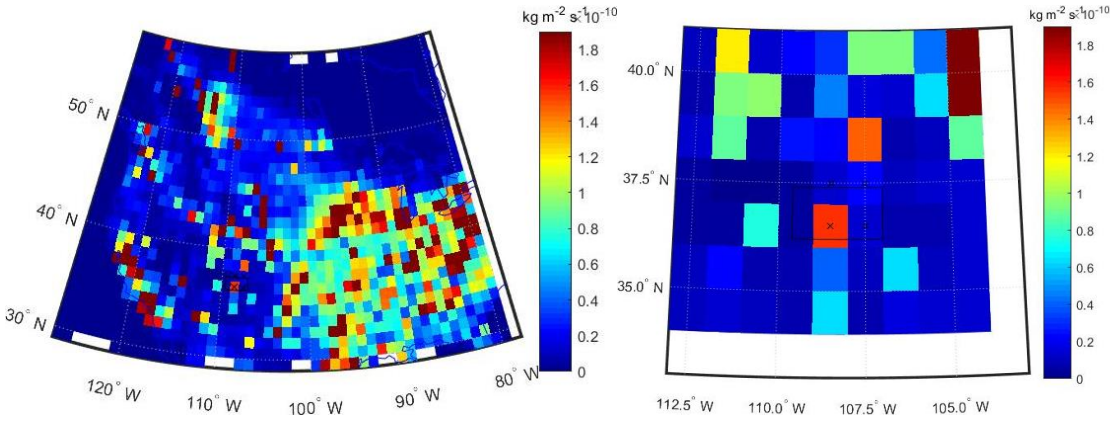

Figure 22. EDGAR draft v4.3.2 total CH_4 emission for 4C in 2008. Resolution: 1°×1°.

Table 14. EDGAR draft v4.3.2 CH_4 emissions from the 4C source area, and the source area + surrounding grid-cells.

4C	Surrounding	Source	Surrounding	Source
Area (km^2)	157919	39549		
EDGAR category	Avg ($kg \cdot m^{-2} \cdot s^{-1}$)	Avg ($kg \cdot m^{-2} \cdot s^{-1}$)	Total ($Tg \cdot yr^{-1}$)	Total ($Tg \cdot yr^{-1}$)
Agricultural soils	0	0	0	0
Agricultural waste burning	4.39×10^{-15}	3.41×10^{-15}	2.19×10^{-5}	4.26×10^{-6}
Production of chemicals	1.54×10^{-14}	1.57×10^{-15}	7.70×10^{-5}	1.97×10^{-6}
Energy industry	1.12×10^{-13}	4.08×10^{-13}	0.000558	0.000510
Enteric fermentation	5.66×10^{-12}	5.42×10^{-12}	0.0283	0.00678
Fossil fuel fires	7.56×10^{-13}	3.02×10^{-12}	0.00377	0.00378
Manufacturing Industry	2.12×10^{-14}	2.12×10^{-15}	0.000106	2.65×10^{-6}
Production of iron and steel	0	0	0	0
Large scale biomass burning	1.36×10^{-14}	1.82×10^{-14}	6.78×10^{-5}	2.28×10^{-5}
Manure management	5.75×10^{-13}	5.51×10^{-13}	0.00287	0.000689
Fuel combustion and production	2.36×10^{-11}	4.11×10^{-11}	0.118	0.0514
Residential	1.87×10^{-13}	1.18×10^{-13}	0.000934	0.000147
Oil refineries, transformation industry	2.27×10^{-14}	3.20×10^{-14}	0.000114	4.00×10^{-5}
Solid waste disposal	2.88×10^{-12}	1.44×10^{-14}	0.0144	1.80×10^{-5}
Non-road transport	6.68×10^{-15}	5.19×10^{-15}	3.33×10^{-5}	6.49×10^{-6}
Road transport	2.27×10^{-13}	2.32×10^{-13}	0.00113	0.000291
Waste water	6.02×10^{-13}	1.64×10^{-13}	0.00301	0.000206
Total	3.47×10^{-11}	5.11×10^{-11}	0.173	0.0639
Our source emission ($Tg \cdot yr^{-1}$)			0.62±0.30	

3.2.4. Regridded South Shānxī

The area is shown in Figure 6. Now we are going to do the emission estimation again with the new method we develop in this research.

SCIAMACHY observation

The SCIAMACHY XCH_4 data averaged from 2003 to 2009 is shown at $1° \times 1°$ resolution in Figure 23. The grid-cell with the highest XCH_4 value is defining the SS source area.

Elevation corrected SCIAMACHY observation

The elevation corrected SS region is shown in Figure 23.

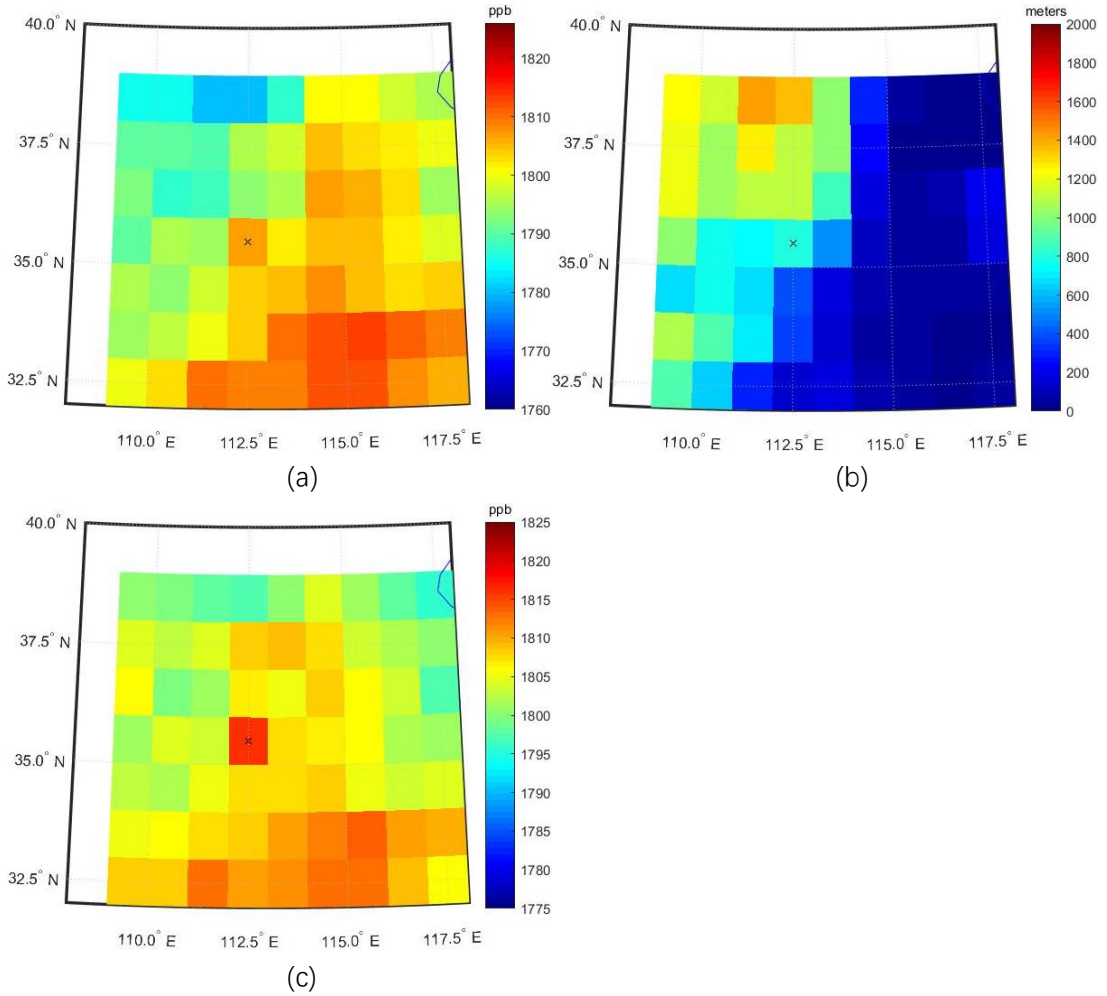

Figure 23. SS region at 1°×1°. (a) shows the SCIAMACHY XCH_4 data averaged from 2003 to 2009. (b) shows the average ground pixel elevation. (c) shows the SCIAMACHY XCH_4 data averaged from 2003 to 2009 after the elevation correction. The black cross marks the SS source area.

ΔXCH_4

20% of all grid cells with the lowest XCH_4 values are chosen for the background analysis, in the small, medium and large sizes respectively. It is shown in Figure 24.

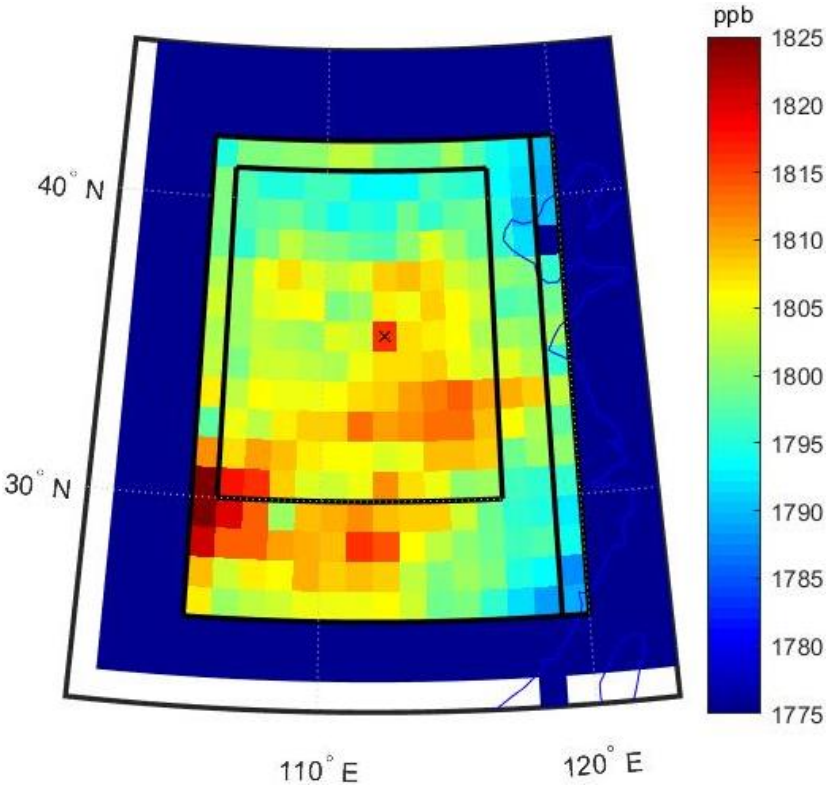

Figure 24. Background analysis of SS. The three thick black squares represent the small, medium, large sizes for background analysis. 20% of the grid cells inside the squares with lowest XCH_4 values are chosen. The black cross represents the hotspot region.

Table 15. Results for SS source background analysis (unit: ppb).

	XCH_4	1σ uncertainty
Source	1815.75	2.36
Background small	1796.15	0.38
Background medium	1795.35	0.30
Background large	1794.39	0.31
Difference small	19.60	2.39
Difference medium	20.40	2.38
Difference large	21.36	2.38

From Table 15, we can see the XCH_4 values among different sizes vary slightly. So, we choose the one with the smallest uncertainty, which is background large in this case. The ΔXCH_4 is 21.36±2.38 ppb.

ΔEMI

The modeled plume for a single grid cell in the SS region is shown in Table 16.

Table 16. Average XCH_4 on 5×5 grid, output of TM5 forward run for the year 2014, units (ppb), at 1°×1° resolution. The center of the center cell is located at lat 35.5°N and lon 112.5°E. The input is an emission of 1 $Tg \cdot yr^{-1}$ by the center grid-cell and no emission from the surrounding cells.

1.59	1.89	2.08	2.34	1.97
1.91	2.73	4.59	4.08	2.69
2.36	5.67	13.90	6.76	3.34
2.45	4.26	5.50	4.15	3.35
2.08	2.54	2.51	2.60	2.64

ΔXCH_4 for an emission of 1 $Tg \cdot yr^{-1}$ for the SS hotspot according to the model is 13.90±1.50 ppb. ΔXCH_4 according to SCIAMACHY is 21.36±2.38 ppb. Therefore ΔEMI of the source grid cell in the source area is 21.36/13.90=1.54±0.24 $Tg \cdot yr^{-1}$.

EMI

Note that ΔEMI is with respect to SS background large. For EMI of the source area a background emission must be added. The average emission of SS background large is 3.42×10^{-10} $kg \cdot m^{-2} \cdot s^{-1}$ according to EDGAR draft v4.3.2 'total'. The total area of the source area is 10067 km^2. Hence the background emission (*EMI_background*) of the 4C source area is 0.109 $Tg \cdot yr^{-1}$. Note that this background emission is only 7.1% of ΔEMI. The EMI of the source area is therefore 1.65±0.24 $Tg \cdot yr^{-1}$.

Applying the correction factor

In subsection 3.2.3, it is determined that the emissions are over-estimated by a factor of 4.28 ±2.05. Applying this correction factor to SS, we get an emission rate of 1.65/4.28=0.39±0.20 $Tg \cdot yr^{-1}$.

Comparison to EDGAR

EDGAR draft v4.3.2 'total' is shown in Figure 25.
The tabulated information for SS source and SS source + immediate surrounding is shown in Table 17. It shows the highest and dominant source sector is hard coal. However, the difference of emission estimations between EDGAR and our method is significant, around 1.61/0.41=3.93 times. It might be because of the coarse resolution, or the inaccuracy of EDGAR inventory, or the insufficiency of elevation correction on SCIAMACHY data.

Table 17. EDGAR draft v4.3.2 CH_4 emissions from the SS source area, and the source area + surrounding grid-cells.

SS	Surrounding	Source	Surrounding	Source
Area (km^2)	90579	10067		
EDGAR category	Avg ($kg \cdot m^{-2} \cdot s^{-1}$)	Avg ($kg \cdot m^{-2} \cdot s^{-1}$)	Total ($Tg \cdot yr^{-1}$)	Total ($Tg \cdot yr^{-1}$)
Agricultural soils	9.77×10^{-12}	1.31×10^{-12}	0.0280	0.000418
Agricultural waste burning	1.26×10^{-13}	8.89×10^{-14}	0.000361	2.83×10^{-5}
Production of chemicals	8.07×10^{-13}	3.55×10^{-13}	0.00231	0.000113
Energy industry	5.64×10^{-13}	8.59×10^{-13}	0.00161	0.000274
Enteric fermentation	7.28×10^{-11}	5.23×10^{-11}	0.208	0.0167
Fossil fuel fires	1.10×10^{-12}	1.65×10^{-12}	0.00316	0.000525
Manufacturing Industry	1.47×10^{-12}	1.08×10^{-12}	0.00420	0.000345
Production of iron and steel	4.33×10^{-14}	0	0.000124	0
Large scale biomass burning	1.45×10^{-14}	5.38×10^{-15}	4.17×10^{-5}	1.71×10^{-6}
Manure management	1.21×10^{-11}	7.70×10^{-12}	0.0347	0.00245
Fuel combustion and production	1.64×10^{-9}	4.03×10^{-9}	4.71	1.28
Residential	4.73×10^{-11}	3.33×10^{-11}	0.136	0.0106
Oil refineries, transformation industry	1.28×10^{-12}	1.06×10^{-13}	0.00368	3.38×10^{-5}
Solid waste disposal	3.10×10^{-11}	1.36×10^{-11}	0.0889	0.00433
Non-road transport	2.95×10^{-14}	1.01×10^{-14}	8.45×10^{-5}	3.20×10^{-6}
Road transport	6.91×10^{-13}	3.84×10^{-13}	0.00198	0.000122
Waste water	8.04×10^{-11}	4.89×10^{-11}	0.230	0.0156
Total	1.90×10^{-9}	4.19×10^{-9}	5.45	1.33
Our source emission ($Tg \cdot yr^{-1}$)			0.39±0.20	

3.3. Result Summaries

In our research, two hotspots, 4C and SS are analyzed, with both a normal gridding method and a new gridding method. The 4C hotpot is used as validation. The SS hotpot was found out in previous research, which is studies in our research to verify the emission estimation method.

The latest EDGAR edition, draft v4.3.2 2008, is used for comparison and background analyses.

Table 18. Summary of emissions before applying the correction factor.

Area	ΔXCH_4 (ppb)	ΔEMI ($Tg \cdot yr^{-1}$)	EMI_background ($Tg \cdot yr^{-1}$)	EMI ($Tg \cdot yr^{-1}$)
4C	17.08±0.84	2.40±0.18	0.039	2.44±0.21
SS	23.56±1.70	1.69±0.22	0.112	1.80±0.22
4C (regridded)	16.58±1.24	2.60±0.24	0.040	2.64±0.24
SS (regridded)	21.36±2.38	1.54±0.24	0.109	1.65±0.24

Table 19. Summary of emissions determined from the hotpots.

Area	Our emission ($Tg \cdot yr^{-1}$)	EDGAR draft v4.3.2 2008 emission ($Tg \cdot yr^{-1}$)	Emission of *J. W., 2016* ($Tg \cdot yr^{-1}$)	EDGAR v4.2 2008 emission ($Tg \cdot yr^{-1}$)	Surface area ($10^3 km^2$)
4C	0.58±0.24	0.06	0.65 ± 0.27	0.19	30
SS	0.43±0.18	1.34	0.31 ± 0.14	0.06	10
4C (regridded)	0.62±0.30	0.06	-	-	40
SS (regridded)	0.39±0.20	1.34	-	-	10

4. Discussions

4.1. Elevation Correction

In the calculation process of TM5 model-derived global elevation correction matrix, there is no averaging kernel from SCIAMACHY data used, since the SCIAMACHY data here are only available over the land. However, the elevation correction matrix derived from TM5 model requires data all over the earth surface. If the satellite data over the ocean are also available, in theory, the matrix combined with SCIAMACHY satellite averaging kernels will not require the validation from local elevation correction results (shown in Figure 11), which are not always reliable due to the unknown local anthropogenic methane emission sources.

The elevation correction method used in this research makes use of a linear relationship. However, the elevation corrected SCIAMACHY data (Figure 13) show areas where the elevation dependence of XCH_4 is not reduced but increased, such as over the Tibetan Plateau, Antarctic and Greenland. On the spatial resolution of our analysis, the Tibetan Plateau has the

highest surface elevation on Earth. Antarctic and Greenland have very high altitudes and latitudes. It shows the linear elevation correction does not work well in high altitudes (e.g. 3km above the earth surface) and latitudes.

4.2. Background Selection and ΔXCH_4

In our research, 20% of all the grid cells in the surrounding areas with lowest ΔXCH_4 are chosen to calculate the background emissions. However, there is still a certain degree of possibility that the unknown local sources will influence the background emission estimation. These influences can be varied in support of the uncertainty quantification.

4.3. Validation to Four Corners Region

In our research, we validate our estimated emission to 4C region to derive an over-estimation factor. However, the paper we referred to is from *Kort et al., 2014*, which uses a partially different area and a different emission inventory. In our research, we adjust the validation number by keeping the ground-based measurements from *Kort et al.*'s paper, to determine the validation number; adjust the error on the validation number based on partially different areas. The switch between the two EDGAR inventory editions does not matter significantly since the background emission only takes a small part of the total emission. Further research with ground-based measurements is required. SCIAMACHY is intrinsically limited in its ability to resolve local sources, because of its large footprint. Other instruments will be launched soon (TROPOMI planned on 21st September 2017) that measures at much higher resolution, which will facilitate this problem.

4.4. The Hotspot Determination

After the regridding, we find one more hotspot appears in the 4C region. However, our method to look for hotspots is not precise. Since with different color bars, the color differences can be different. when there is a gradual color change of grid cells around the hotspot areas, the determination of the hotspot locations becomes intrigues as well. It will be more scientific to set up a quantified system for deciding what and where are the hotspot cells in the map after the elevation correction. One way might be to model the background with a high-resolution model, and assess the difference with what the satellite is seeing. But one would still have to check the statistics of the differences to avoid ending up classifying outliers as local sources.

All hotspots are simulated as a single uniformed emitting source. However, if there are also other emitting sources around, the simulation will lead to an over estimate of the strength of the hotspot. Since it is modeled as all the emission comes from an only source. In East China, the unknown emission is hard to determine and locate, which brings uncertainties on the simulated results.

Right now, the model has zero emission everywhere else. This is a very simplistic starting point.

It is better is to combine this with a simulation of the background concentration. The motivation for the current approach is that if the emission inventory is bad the background may not be much better simulated than the one subtracted from the SCIAMACHY data. In case of isolated sources, the approach in this research may not be so bad. However, for more complicated cases a better one is needed.

4.5. The Verification of Emission Estimation and Regridding Method

Due to the lack of ground-based measurements in SS hotspot, the estimation results cannot be verified. It makes the comparison between the normal gridding and the new gridding methods hard. But it still serves the uncertainty assessment. The uncertainty quantification method is overall accurate in this research. With a certain local emission estimation, some more conclusions about which gridding way is better will come up. We need a known target to develop the methods.

5. Conclusions

The aims of this research are to quantify anthropogenic emissions of methane from large local sources using satellite data, and compare methane emissions estimated using top down (satellite) and bottom up (statistical inventories) approaches. This research with SCIAMACHY satellite data can be preparation for the new satellite mission S5p TROPOMI (planned at 21st Sept. 2017).

In our research, a global orographic correction matrix is derived based on TM5 model, with two variables, time and latitude. It works well on showing the large local sources by decreasing the influence of surface elevation variations. The matrix is calibrated with the SCIAMACHY satellite data around 4C and Middle East, so it is most suitable for mid latitude regions. This matrix can be applied to other regions for doing elevation correction as well, but with a new local data validation based on specific latitude ranges. The matrix is based on TM5 model, which gets rid of the influences of local unknown emission sources and makes it better to use for the whole globe, especially in industrialized regions without reliable ground-based measurements.

The new gridding method changes the hotspot area in 4C region, but works almost the same when determining the hotspot location around the SS region. The emission quantification results from the new gridding method have no significant difference with the normal gridding method, which means the two gridding methods keep consistent and the results are robust. However, according to TCCON measurements, the normal gridding method is more accurate on locating emission sources in 4C region, since the extra hotspot grid cell after the new gridding method does not exist in TCCON measurement. The new gridding method makes the error values bigger in every step of emission estimations. Since values of results keep consistent, normal gridding is better for simpler and faster calculations. The insufficiency of

the new gridding method in this research probably depends on resolution.

The quantification results in 4C are relatively good, since it basically keeps consistent with the ground-based measurement in TCCON in that area, which is ~0.59 $Tg \cdot yr^{-1}$. In SS, our emission estimation result is ~7.2 times (normal gridding method), ~6.5 times (new gridding method) of EDGAR v4.2 (0.06 $Tg \cdot yr^{-1}$), and ~1.4 times (normal gridding method), ~1.3 times (new gridding method) of the estimation result in J. W. (2016)'s paper (0.31±0.14 $Tg \cdot yr^{-1}$). With the lack of ground-based measurements in that region, it is hard to determine the true methane emission per year. However, In the latest EDGAR draft v4.3.2, the local emission around SS hotspot is ~22.3 times of EDGAR v4.2, so an increase of the emission estimation is beneficial. The estimated values in EDGAR draft v4.3.2 are possible to be overestimated according to our results.

References

Frankenberg C, Meirink J F, Bergamaschi P, et al. Satellite chartography of atmospheric methane from SCIAMACHY on board ENVISAT: Analysis of the years 2003 and 2004[J]. Journal of Geophysical Research: Atmospheres, 2006, 111(D7).

Peters W, Jacobson A R, Sweeney C, et al. An atmospheric perspective on North American carbon dioxide exchange: CarbonTracker[J]. Proceedings of the National Academy of Sciences, 2007, 104(48): 18925-18930.

Frankenberg C, Aben I, Bergamaschi P, et al. Global column-averaged methane mixing ratios from 2003 to 2009 as derived from SCIAMACHY: Trends and variability[J]. Journal of Geophysical Research: Atmospheres, 2011, 116(D4).

Goody R M, Yung Y L. Atmospheric radiation: theoretical basis[M]. Oxford University Press, 1995.

Kort E A, Frankenberg C, Costigan K R, et al. Four corners: The largest US methane anomaly viewed from space[J]. Geophysical Research Letters, 2014, 41(19): 6898-6903.

'Technical summary'. *Climate Change 2001. United Nations Environment Programme.*

Wunch D, Toon G C, Blavier J F L, et al. The total carbon column observing network[J]. Philosophical Transactions of the Royal Society of London A: Mathematical, Physical and Engineering Sciences, 2011, 369(1943): 2087-2112.

Bovensmann H, Burrows J P, Buchwitz M, et al. SCIAMACHY: Mission objectives and measurement modes[J]. Journal of the atmospheric sciences, 1999, 56(2): 127-150.

Connor B J, Kuang Z, Toon G C, et al. The Averaging Kernel of CO2 column measurements by the Orbiting Carbon Observatory (OCO), Its Use in Inverse Modeling, and Comparisons to AIRS, SCIAMACHY, and ground-based FTIR[C]//AGU Fall Meeting Abstracts. 2003.

Patra P K, Houweling S, Krol M, et al. TransCom model simulations of CH 4 and related species: linking transport, surface flux and chemical loss with CH 4 variability in the troposphere and lower stratosphere[J]. Atmospheric Chemistry and Physics, 2011, 11(24): 12813-12837.